

# Addressing the LHC 750 GeV diphoton excess without new colored states

Amine Ahriche,<sup>1, 2, 3, \*</sup> Gaber Faisel,<sup>2, 4, 5, †</sup> Salah Nasri,<sup>6, ‡</sup> and Jusak Tandean<sup>2, §</sup>

<sup>1</sup>*Laboratory of Mathematical and Sub-Atomic Physics (LPMPS),  
University of Constantine I, DZ-25000 Constantine, Algeria.*

<sup>2</sup>*Department of Physics and Center for Theoretical Sciences,  
National Taiwan University, Taipei 106, Taiwan.*

<sup>3</sup>*The Abdus Salam International Centre for Theoretical Physics,  
Strada Costiera 11, I-34014, Trieste, Italy.*

<sup>4</sup>*Department of Physics, Faculty of Arts and Sciences,  
Süleyman Demirel University, Isparta, Turkey 32260.*

<sup>5</sup>*Egyptian Center for Theoretical Physics,  
Modern University for Information and Technology, Cairo 11212, Egypt.*

<sup>6</sup>*Department of Physics, United Arab Emirates University, Al-Ain, UAE.*

## Abstract

The modest excess in the diphoton invariant mass spectrum around 750 GeV recently detected at the LHC could be preliminary evidence for the existence of a heavy new resonance. Assuming that it is a spinless boson, dubbed  $\tilde{s}$ , we consider it within a model containing two weak scalar doublets having zero vacuum expectation values and a scalar singlet in addition to the doublet responsible for breaking the electroweak symmetry. We show that the model is consistent with all phenomenological constraints and can yield a production cross section  $\sigma(pp \rightarrow \tilde{s} \rightarrow \gamma\gamma)$  of roughly the desired size, mainly via the photon-fusion contribution, without involving extra colored fermions or bosons. We also discuss other major decay modes of  $\tilde{s}$  which are potentially testable in upcoming LHC measurements.

---

\*Electronic address: aahrache@ictp.it

†Electronic address: gfaisel@hep1.phys.ntu.edu.tw

‡Electronic address: snasri@uaeu.ac.ae

§Electronic address: jtandean@yahoo.com

## I. INTRODUCTION

The most recent data collected at the LHC from proton-proton collisions at a center-of-mass energy of  $\sqrt{s} = 13$  TeV have turned up tantalizing potential hints of physics beyond the standard model (SM). Specifically, upon searching for new resonances decaying into two photons, the ATLAS and CMS Collaborations [1, 2] have reported observing modest excesses above the backgrounds peaked at a mass value of around 750 GeV with local (global) significances of  $3.9\sigma$  and  $3.4\sigma$  ( $2.1\sigma$  and  $1.6\sigma$ ), respectively [3, 4]. If interpreted as telltales of a resonance, the ATLAS data suggest that it has a width of about 50 GeV, whereas the CMS results prefer it to be narrower [3, 4]. As pointed out in a number of theoretical works [5] appearing very shortly after the ATLAS and CMS announcements [1, 2], the cross section of producing the putative heavy particle decaying into  $\gamma\gamma$  falls within the range of roughly 2-13 fb, and it is possible for its width to be less than 50 GeV or even narrow.

Given the limited statistics of the diphoton excess events, it would still be premature to hold a definite view concerning these findings. Nevertheless, if the tentative indications of the existence of a non-SM state are confirmed by upcoming measurements, the acquired data will not only constitute more conclusive evidence for new physics, but also paint a clearer picture of the new particle's properties which will then serve as a test for models. It is therefore of interest in the meantime to explore a variety of new-physics scenarios that can accommodate it, subject to the relevant available experimental constraints, and also to look at other aspects of these recent LHC results [5-11].

Here we consider the possibility that the excess diphoton events proceeded from the decay of a new spinless boson, which we denote by  $\tilde{s}$  and arises due to the presence of a complex scalar field,  $\zeta$ , transforming as a singlet under the SM gauge group,  $SU(2)_L \times U(1)_Y$ . In our scenario of interest, the scalar fields also include two new weak doublets,  $\eta_1$  and  $\eta_2$ , having zero vacuum expectation values (VEVs), besides the doublet,  $\Phi$ , which contains the Higgs boson in the SM. Furthermore, the gauge sector is somewhat expanded in comparison to that of the SM by the addition of a new Abelian gauge symmetry,  $U(1)_D$ , under which  $\zeta$  and  $\eta_{1,2}$  are charged, while SM particles are not. Consequently,  $\eta_{1,2}$  have no direct interactions with a pair of exclusively SM fermions, whereas  $\tilde{s}$  can couple at tree level to the latter because of mixing between the remaining components of  $\zeta$  and  $\Phi$  after they develop nonzero VEVs. Having no VEVs nor couplings to SM fermion pairs,  $\eta_{1,2}$  have been termed inert in the literature [12], but being weak doublets they do interact directly with SM gauge bosons. For simplification, we suppose that the  $U(1)_D$  gauge boson has vanishing kinetic mixing with the hypercharge gauge boson, and thus the former can be regarded as dark. It is worth noting that in the absence of the singlet,  $\zeta$ , the model corresponds to one of the possible three-scalar-doublet cases catalogued in Ref. [12] and has been examined for its interesting potential impact on the Higgs trilinear coupling and electroweak phase transition in Ref. [13].

The remainder of the paper is organized as follows. In the next section, we describe the salient features of the model and the scalar particles' interactions of concern and masses. In Sec. III, we enumerate the major decay modes of  $\tilde{s}$ . In Sec. IV, we discuss constraints on the scalars from theoretical requirements, electroweak precision data, and collider measurements. We present our numerical analysis in Sec. V, demonstrating that the model can generate the requisite LHC

values of the production cross-section  $\sigma(pp \rightarrow \tilde{s} \rightarrow \gamma\gamma)$  mainly via the photon-fusion contribution. Hence our scenario does not involve any colored fermions or bosons to enhance the  $\tilde{s}\gamma\gamma$  coupling. Also, we briefly discuss what other decay modes of  $\tilde{s}$  and additional signatures of the model may be checked experimentally in order to probe the model more stringently. We give our conclusions in Sec. VI. Some complementary information and formulas are relegated to an appendix.

## II. MODEL

The quantum numbers of the scalar fields are listed in Table I. Accordingly, we can express the Lagrangian describing their renormalizable interactions with each other and with the SM gauge bosons,  $W_j$  and  $B$ , and the  $U(1)_D$  gauge boson  $C$  as

$$\mathcal{L} = (\mathcal{D}^\rho \Phi)^\dagger \mathcal{D}_\rho \Phi + (\mathcal{D}^\rho \eta_a)^\dagger \mathcal{D}_\rho \eta_a + (\mathcal{D}^\rho \zeta)^\dagger \mathcal{D}_\rho \zeta - \mathcal{V}, \quad (1)$$

$$\mathcal{D}^\rho \Delta = (\partial^\rho + \frac{i}{2} g \tau_j W_j^\rho + i g_Y \mathcal{Q}_Y B^\rho + i g_D \mathcal{Q}_C C^\rho) \Delta, \quad \Delta = \Phi, \eta_1, \eta_2,$$

$$\mathcal{D}^\rho \zeta = (\partial^\rho + i g_D \mathcal{Q}_C C^\rho) \zeta, \quad \mathcal{Q}_C(\Phi, \eta_1, \eta_2, \zeta) = (0, \eta_1, -\eta_2, 2\zeta),$$

$$\begin{aligned} \mathcal{V} = & \mu_1^2 \Phi^\dagger \Phi + \mu_{2a}^2 \eta_a^\dagger \eta_a + \mu_\zeta^2 |\zeta|^2 + \frac{1}{2} \lambda_1 (\Phi^\dagger \Phi)^2 + \frac{1}{2} \lambda_{2a} (\eta_a^\dagger \eta_a)^2 + \frac{1}{2} \lambda_\zeta |\zeta|^4 \\ & + \lambda_{3a} \Phi^\dagger \Phi \eta_a^\dagger \eta_a + \lambda_{3\zeta} \Phi^\dagger \Phi |\zeta|^2 + \lambda_{4a} \Phi^\dagger \eta_a \eta_a^\dagger \Phi + \frac{1}{2} (\lambda_5 \Phi^\dagger \eta_1 \Phi^\dagger \eta_2 + \text{H.c.}) \\ & + \lambda_6 \eta_1^\dagger \eta_1 \eta_2^\dagger \eta_2 + \lambda_7 \eta_1^\dagger \eta_2 \eta_2^\dagger \eta_1 + \lambda_{a\zeta} \eta_a^\dagger \eta_a |\zeta|^2 + (\mu_{\eta\zeta} \eta_1^\dagger \eta_2 \zeta + \text{H.c.}), \end{aligned} \quad (2)$$

where  $g_D$  and  $\mathcal{Q}_C$  are the coupling constant and charge operator of  $U(1)_D$ , respectively, summation over  $a = 1, 2$  and  $j = 1, 2, 3$  is implicit and, after electroweak symmetry breaking, in the unitary gauge

$$\Phi = \begin{pmatrix} 0 \\ \frac{1}{\sqrt{2}}(v + \phi) \end{pmatrix}, \quad \eta_a = \begin{pmatrix} \eta_a^+ \\ \eta_a^0 \end{pmatrix}, \quad \eta_a^0 = \frac{\text{Re } \eta_a^0 + i \text{Im } \eta_a^0}{\sqrt{2}}, \quad \zeta = \frac{\tilde{v} + \zeta}{\sqrt{2}}, \quad (3)$$

with  $v$  and  $\tilde{v}$  denoting the vacuum expectation values (VEVs) of  $\Phi$  and  $\zeta$ , respectively. The Hermiticity of  $\mathcal{V}$  implies that  $\mu_{1,2a,\zeta}^2$  and  $\lambda_{1,2a,3a,4a,6,7,\zeta,3\zeta,a\zeta}$  must be real. Since the phases of  $\eta_{1,2}$  relative to  $\Phi$  and  $\zeta$  can be arranged to render  $\lambda_5$  and  $\mu_{\eta\zeta}$  real, without loss of generality we will choose these parameters to be real.

One can see from Eq. (1) that, after  $\Phi$  and  $\zeta$  develop nonzero VEVs, their remaining components  $\phi$  and  $\zeta$ , respectively, generally mix with each other. Moreover, the  $\mu_{\eta\zeta}$  terms break  $U(1)_D$  into  $\mathcal{Z}_2$  under which all the inert scalars are odd, as Table I indicates, and all the other fields

	$\Phi$	$\eta_1$	$\eta_2$	$\zeta$
$SU(2)_L$	2	2	2	1
$U(1)_Y$	1/2	1/2	1/2	0
$U(1)_D [Z_2]$	0 [+]	1 [-]	-1 [-]	2 [+]

TABLE I: Charge assignments of the scalars in the model.

even. We remark that, although the lightest of the electrically neutral  $\mathcal{Z}_2$ -odd scalars are stable, we find that in our parameter space of interest they cannot serve as good candidates for dark matter (DM). This is because they annihilate into SM particles too fast due to their tree-level interactions with SM gauge and Higgs bosons and hence cannot produce enough relic abundance. To reproduce the observed relic abundance, one needs to have a more complete model, but we assume that the extra ingredients responsible for explaining DM have negligible or no impact on our scalar sector of interest, so that they do not affect the results of this study.

After the  $U(1)_D \rightarrow \mathcal{Z}_2$  breaking, the  $\mu_{\eta\zeta}$  terms also induce the mixing of  $\mathcal{Z}_2$ -odd scalars of the same electric charge. To examine this more closely, we can write the part of  $\mathcal{L}$  from  $\mathcal{V}$  which is quadratic in the scalar fields as

$$\mathcal{L} \supset -\frac{1}{2} (\phi \quad \zeta) M_{\phi\zeta}^2 \begin{pmatrix} \phi \\ \zeta \end{pmatrix} - (\eta_1^- \quad \eta_2^-) M_{\mathcal{C}}^2 \begin{pmatrix} \eta_1^+ \\ \eta_2^+ \end{pmatrix} - \frac{1}{2} \eta_0^T M_0^2 \eta_0, \quad (4)$$

where the expressions for the matrices  $M_{\phi\zeta}^2$ ,  $M_{\mathcal{C}}^2$ ,  $M_0^2$ , and  $\eta_0$  can be found in Appendix A.

Upon diagonalizing  $M_{\phi\zeta}^2$ , we obtain the mass eigenstates  $h$  and  $\tilde{s}$  and their respective masses  $m_h$  and  $m_{\tilde{s}}$  given by

$$\begin{aligned} \begin{pmatrix} \phi \\ \zeta \end{pmatrix} &= \begin{pmatrix} c_\xi & s_\xi \\ -s_\xi & c_\xi \end{pmatrix} \begin{pmatrix} h \\ \tilde{s} \end{pmatrix} \equiv \mathcal{O}_{\phi\zeta} \begin{pmatrix} h \\ \tilde{s} \end{pmatrix}, \quad c_\xi = \cos \xi, \quad s_\xi = \sin \xi, \\ \mathcal{O}_{\phi\zeta}^T M_{\phi\zeta}^2 \mathcal{O}_{\phi\zeta} &= \text{diag}(m_h^2, m_{\tilde{s}}^2), \\ 2m_{h,\tilde{s}}^2 &= m_\phi^2 + m_\zeta^2 \mp \sqrt{(m_\phi^2 - m_\zeta^2)^2 + m_{\phi\zeta}^4}, \quad \tan(2\xi) = \frac{m_{\phi\zeta}^2}{m_\zeta^2 - m_\phi^2}, \\ m_\phi^2 &= \lambda_1 v^2, \quad m_\zeta^2 = \lambda_\zeta \tilde{v}^2, \quad m_{\phi\zeta}^2 = 2\lambda_{3\zeta} v\tilde{v}. \end{aligned} \quad (5)$$

It follows that  $m_h \sim 125$  GeV and  $m_{\tilde{s}} \sim 750$  GeV. Furthermore, all the tree-level couplings of  $h$  ( $\tilde{s}$ ) to SM fermions and weak bosons,  $W$  and  $Z$ , are  $c_\xi$  ( $s_\xi$ ) times the corresponding SM Higgs couplings.

For the electrically charged inert scalars, from the  $M_{\mathcal{C}}^2$  term in Eq. (4), we arrive at the mass eigenstates  $H_{1,2}^\pm$  and their masses  $m_{H_1, H_2}$  given by

$$\begin{aligned} \begin{pmatrix} \eta_1^+ \\ \eta_2^+ \end{pmatrix} &= \begin{pmatrix} c_H & s_H \\ -s_H & c_H \end{pmatrix} \begin{pmatrix} H_1^+ \\ H_2^+ \end{pmatrix} \equiv \mathcal{U}_{\mathcal{C}} \begin{pmatrix} H_1^+ \\ H_2^+ \end{pmatrix}, \quad c_H = \cos \theta_H, \quad s_H = \sin \theta_H, \\ \mathcal{U}_{\mathcal{C}}^\dagger M_{\mathcal{C}}^2 \mathcal{U}_{\mathcal{C}} &= \text{diag}(m_{H_1}^2, m_{H_2}^2), \quad m_{H_a} \equiv m_{H_a^\pm}, \\ 2m_{H_1, H_2}^2 &= m_{c_1}^2 + m_{c_2}^2 \mp \sqrt{(m_{c_1}^2 - m_{c_2}^2)^2 + m_{c\zeta}^4}, \quad \tan(2\theta_H) = \frac{m_{c\zeta}^2}{m_{c_2}^2 - m_{c_1}^2}, \end{aligned} \quad (6)$$

where  $m_{c_a, c\zeta}^2$  are related to other parameters in Eq. (A1) and we have taken  $\mu_{\eta\zeta}$ , and hence  $m_{c\zeta}^2$ , to be real. Similarly, the mixing of the electrically neutral inert scalars gives rise to the mass

eigenstates  $\mathcal{S}_a$  and  $\mathcal{P}_a$  with their respective masses  $m_{\mathcal{S}_a}$  and  $m_{\mathcal{P}_a}$  according to

$$\begin{pmatrix} \text{Re } \eta_1^0 \\ \text{Re } \eta_2^0 \\ \text{Im } \eta_1^0 \\ \text{Im } \eta_2^0 \end{pmatrix} = \begin{pmatrix} c_S & s_S & 0 & 0 \\ -s_S & c_S & 0 & 0 \\ 0 & 0 & c_P & s_P \\ 0 & 0 & s_P & -c_P \end{pmatrix} \begin{pmatrix} \mathcal{S}_1 \\ \mathcal{S}_2 \\ \mathcal{P}_1 \\ \mathcal{P}_2 \end{pmatrix} \equiv \mathcal{O}_0 \begin{pmatrix} \mathcal{S}_1 \\ \mathcal{S}_2 \\ \mathcal{P}_1 \\ \mathcal{P}_2 \end{pmatrix},$$

$$c_S = \cos \theta_S, \quad s_S = \sin \theta_S, \quad c_P = \cos \theta_P, \quad s_P = \sin \theta_P,$$

$$\mathcal{O}_0^T M_0^2 \mathcal{O}_0 = \text{diag} (m_{\mathcal{S}_1}^2, m_{\mathcal{S}_2}^2, m_{\mathcal{P}_1}^2, m_{\mathcal{P}_2}^2),$$

$$2m_{\mathcal{S}_1, \mathcal{S}_2}^2 = m_{n_1}^2 + m_{n_2}^2 \mp \sqrt{(m_{n_1}^2 - m_{n_2}^2)^2 + m_{n\zeta}^4}, \quad \tan(2\theta_S) = \frac{m_{n\zeta}^2}{m_{n_2}^2 - m_{n_1}^2},$$

$$2m_{\mathcal{P}_1, \mathcal{P}_2}^2 = m_{n_1}^2 + m_{n_2}^2 \mp \sqrt{(m_{n_1}^2 - m_{n_2}^2)^2 + \tilde{m}_{n\zeta}^4}, \quad \tan(2\theta_P) = \frac{\tilde{m}_{n\zeta}^2}{m_{n_2}^2 - m_{n_1}^2}, \quad (7)$$

where  $m_{n_a}^2$ ,  $m_{n\zeta}^2$ , and  $\tilde{m}_{n\zeta}^2$  are defined in Eq. (A4). From the last two lines we get

$$m_{\mathcal{S}_1}^2 + m_{\mathcal{S}_2}^2 = m_{\mathcal{P}_1}^2 + m_{\mathcal{P}_2}^2.$$

The simple form of  $\mathcal{O}_0$  above is due to  $\mu_{n\zeta}$  again as well as  $\lambda_5$ , and hence  $m_{n\zeta}^2$  and  $\tilde{m}_{n\zeta}^2$ , being real, which in view of Eq. (A1) also implies that

$$m_{n\zeta}^2 = \tilde{m}_{n\zeta}^2 + 2m_{c\zeta}^2.$$

The kinetic portion of  $\mathcal{L}$  in Eq. (1) contains the interactions of the scalars with the SM gauge bosons,

$$\begin{aligned} \mathcal{L} \supset & \frac{g}{2} \{ [(c_H c_S + s_H s_S) (iH_1^+ \overset{\leftrightarrow}{\partial}^\mu \mathcal{S}_1 + iH_2^+ \overset{\leftrightarrow}{\partial}^\mu \mathcal{S}_2) \\ & + (c_H s_S - s_H c_S) (iH_1^+ \overset{\leftrightarrow}{\partial}^\mu \mathcal{S}_2 - iH_2^+ \overset{\leftrightarrow}{\partial}^\mu \mathcal{S}_1) \\ & + (c_H c_P - s_H s_P) (H_1^+ \overset{\leftrightarrow}{\partial}^\mu \mathcal{P}_1 - H_2^+ \overset{\leftrightarrow}{\partial}^\mu \mathcal{P}_2) \\ & + (c_H s_P + s_H c_P) (H_1^+ \overset{\leftrightarrow}{\partial}^\mu \mathcal{P}_2 + H_2^+ \overset{\leftrightarrow}{\partial}^\mu \mathcal{P}_1)] W_\mu^- + \text{H.c.} \} \\ & + \frac{g}{2c_w} [(c_S c_P - s_S s_P) (\mathcal{P}_1 \overset{\leftrightarrow}{\partial}^\mu \mathcal{S}_1 - \mathcal{P}_2 \overset{\leftrightarrow}{\partial}^\mu \mathcal{S}_2) \\ & + (c_S s_P + s_S c_P) (\mathcal{P}_1 \overset{\leftrightarrow}{\partial}^\mu \mathcal{S}_2 + \mathcal{P}_2 \overset{\leftrightarrow}{\partial}^\mu \mathcal{S}_1)] Z_\mu \\ & + (iH_1^+ \overset{\leftrightarrow}{\partial}^\mu H_1^- + iH_2^+ \overset{\leftrightarrow}{\partial}^\mu H_2^-) (eA_\mu - g_L Z_\mu) \\ & + (H_1^+ H_1^- + H_2^+ H_2^-) \left[ \frac{g^2}{2} W^{+\mu} W_\mu^- + (eA - g_L Z)^2 \right] \\ & + \frac{g^2}{4} [(c_\xi h + s_\xi \tilde{s} + v)^2 + \mathcal{S}_1^2 + \mathcal{S}_2^2 + \mathcal{P}_1^2 + \mathcal{P}_2^2] \left( W^{+\mu} W_\mu^- + \frac{Z^2}{2c_w^2} \right), \end{aligned} \quad (8)$$

where

$$X \overset{\leftrightarrow}{\partial}^\mu Y = X \partial^\mu Y - Y \partial^\mu X, \quad g_L = \frac{g}{2c_w} (2s_w^2 - 1), \quad c_w = \cos \theta_w = \sqrt{1 - s_w^2}, \quad (9)$$

with  $\theta_w$  being the usual Weinberg angle. These affect the oblique electroweak parameters, to be treated later on.

From Eq. (8), one can see that at tree level the masses of the  $W$  and  $Z$  bosons are related to  $v$  by  $m_W = c_w m_Z = gv/2$ , just as in the SM. Although not displayed, there are also terms for the interactions of  $\eta_a$  with the dark gauge boson  $C$ , from which we obtain its mass to be  $m_C = 2g_D\tilde{v}$ . Numerically, we assume that  $m_C > m_{\tilde{s}}$ . As stated earlier, we also assume that kinetic mixing between the U(1) gauge fields,  $B$  and  $C$ , is vanishing.

Now, from the potential in Eq. (1), we derive

$$\begin{aligned} \mathcal{L} \supset & -\lambda_{hH_aH_a} H_a^+ H_a^- h v - \left[ \frac{1}{2} \lambda_{\tilde{s}hh} h^2 + \lambda_{\tilde{s}H_aH_a} H_a^+ H_a^- + \lambda_{\tilde{s}H_1H_2} (H_1^+ H_2^- + H_2^+ H_1^-) \right] \tilde{s} \tilde{v} \\ & - \left( \frac{1}{2} \lambda_{\tilde{s}\mathcal{S}_a\mathcal{S}_a} \mathcal{S}_a^2 + \frac{1}{2} \lambda_{\tilde{s}\mathcal{P}_a\mathcal{P}_a} \mathcal{P}_a^2 + \lambda_{\tilde{s}\mathcal{P}_1\mathcal{P}_2} \mathcal{P}_1 \mathcal{P}_2 + \lambda_{\tilde{s}\mathcal{S}_1\mathcal{S}_2} \mathcal{S}_1 \mathcal{S}_2 \right) \tilde{s} \tilde{v}, \end{aligned} \quad (10)$$

where summation over  $a = 1, 2$  is implicit and the formulas for the  $\lambda$ 's are given in Appendix A. These couplings determine the amplitudes for  $\tilde{s}$  decays into  $hh$  or a pair of the inert scalars if kinematically allowed and, along with Eq. (8), are pertinent to  $h$  and  $\tilde{s}$  decays into  $\gamma\gamma$  and  $\gamma Z$ . These are some of the prominent decay channels of  $\tilde{s}$ , to which we turn next.

### III. DECAY MODES OF $\tilde{s}$

To examine the most important decay modes of  $\tilde{s}$ , we set its mass to be  $m_{\tilde{s}} = 750$  GeV for definiteness, whereas in the case of  $h$  we assign  $m_h = 125.1$  GeV, in accord with the latest mass determination [14]. Hence  $\tilde{s}$  can decay directly into  $hh$  and, if kinematically permitted, into a pair of the inert scalars. With  $\mathcal{X}$  and  $\mathcal{Y}$  representing the two scalars in the final state, for  $m_{\tilde{s}} > m_{\mathcal{X}} + m_{\mathcal{Y}}$  the decay rate is

$$\Gamma(\tilde{s} \rightarrow \mathcal{X}\mathcal{Y}) = \frac{|\lambda_{\tilde{s}\mathcal{X}\mathcal{Y}} \tilde{v}|^2}{(1 + \delta_{\mathcal{X}\mathcal{Y}}) 16\pi m_{\tilde{s}}^3} \sqrt{(m_{\tilde{s}}^2 - m_{\mathcal{X}}^2 - m_{\mathcal{Y}}^2)^2 - 4m_{\mathcal{X}}^2 m_{\mathcal{Y}}^2}, \quad (11)$$

where the  $\lambda_{\tilde{s}\mathcal{X}\mathcal{Y}}$  expressions for various  $\mathcal{X}\mathcal{Y}$  pairs are collected in Eqs. (A8)-(A12) and  $\delta_{\mathcal{X}\mathcal{Y}} = 1$  (0) if  $\mathcal{X} = \mathcal{Y}$  ( $\mathcal{X} \neq \mathcal{Y}$ ). Thus, for instance,  $\Gamma(\tilde{s} \rightarrow hh) \simeq 1.25 \times 10^{-5} |\lambda_{\tilde{s}hh} \tilde{v}|^2 / \text{GeV}$ . The  $\tilde{s}$  decays into final states containing 3 scalars may also happen, but such channels have relatively much smaller rates due to phase-space suppression and therefore can be neglected.

Because of the  $\phi$ - $\zeta$  mixing as specified in Eq. (5), all the tree-level couplings of  $h$  ( $\tilde{s}$ ) to SM fermions,  $W$ , and  $Z$  are  $c_\xi$  ( $s_\xi$ ) times the corresponding SM Higgs couplings. It follows that, since a SM Higgs boson of mass 750 GeV decays almost entirely into  $W^+W^-$ ,  $ZZ$ ,  $t\bar{t}$  at rates which obey the ratio  $\Gamma(h_{\text{SM}}^{750} \rightarrow W^+W^-) : \Gamma(h_{\text{SM}}^{750} \rightarrow ZZ) : \Gamma(h_{\text{SM}}^{750} \rightarrow t\bar{t}) = 145 : 72 : 30$  and amount to 247 GeV [15], the rates of  $\tilde{s} \rightarrow W^+W^-$ ,  $ZZ$ ,  $t\bar{t}$  conform to the same ratio,

$$\Gamma(\tilde{s} \rightarrow W^+W^-) : \Gamma(\tilde{s} \rightarrow ZZ) : \Gamma(\tilde{s} \rightarrow t\bar{t}) = 145 : 72 : 30, \quad (12)$$

and sum up to

$$\Gamma(\tilde{s} \rightarrow W^+W^-) + \Gamma(\tilde{s} \rightarrow ZZ) + \Gamma(\tilde{s} \rightarrow t\bar{t}) = 247 \text{ GeV } s_\xi^2. \quad (13)$$

Our main channel of interest,  $\tilde{s} \rightarrow \gamma\gamma$ , as well as  $\tilde{s} \rightarrow \gamma Z$ , arise from  $t$ ,  $W$ , and  $H_{1,2}$  loop diagrams, in analogy to  $h \rightarrow \gamma\gamma$  and  $h \rightarrow \gamma Z$ , respectively. In the absence of the singlet scalar,

we have derived the rates of the latter decays in Ref. [13]. Modifying the rate formulas in the presence of  $\tilde{s}$ , we now have

$$\begin{aligned}\Gamma(h \rightarrow \gamma\gamma) &= \frac{\alpha^2 G_F m_h^3}{128\sqrt{2}\pi^3} \left| \frac{4c_\xi}{3} A_{1/2}^{\gamma\gamma}(\kappa_t) + c_\xi A_1^{\gamma\gamma}(\kappa_W) + \sum_{a=1}^2 \frac{\lambda_{hH_a} v^2}{2m_{H_a}^2} A_0^{\gamma\gamma}(\kappa_{H_a}) \right|^2, \\ \Gamma(h \rightarrow \gamma Z) &= \frac{\alpha G_F^2 m_W^2 (m_h^2 - m_Z^2)^3}{64\pi^4 m_h^3} \left| \frac{6 - 16s_w^2}{3c_w} c_\xi A_{1/2}^{\gamma Z}(\kappa_t, \mathbf{z}_t) + c_\xi c_w A_1^{\gamma Z}(\kappa_W, \mathbf{z}_W) \right. \\ &\quad \left. - \frac{1 - 2s_w^2}{c_w} \sum_{a=1}^2 \frac{\lambda_{hH_a} v^2}{2m_{H_a}^2} A_0^{\gamma Z}(\kappa_{H_a}, \mathbf{z}_{H_a}) \right|^2, \quad (14)\end{aligned}$$

where  $\alpha = 1/128$  and  $G_F$  are the usual fine-structure and Fermi constants, respectively, the expressions for the form factors  $A_{0,1/2,1}^{\gamma\gamma,\gamma Z}$  are available from Ref. [16], the  $A_0^{\gamma\gamma,\gamma Z}$  terms originate from the  $H_{1,2}$  loop diagrams,  $\kappa_\beta = 4m_\beta^2/m_h^2$ , and  $\mathbf{z}_\beta = 4m_\beta^2/m_Z^2$ . Accordingly, we can deduce the rates of  $\tilde{s} \rightarrow \gamma\gamma, \gamma Z$  to be

$$\begin{aligned}\Gamma(\tilde{s} \rightarrow \gamma\gamma) &= \frac{\alpha^2 G_F m_{\tilde{s}}^3}{128\sqrt{2}\pi^3} \left| \frac{4s_\xi}{3} A_{1/2}^{\gamma\gamma}(\tilde{\kappa}_t) + s_\xi A_1^{\gamma\gamma}(\tilde{\kappa}_W) + \sum_{a=1}^2 \frac{\lambda_{\tilde{s}H_a} v \tilde{v}}{2m_{H_a}^2} A_0^{\gamma\gamma}(\tilde{\kappa}_{H_a}) \right|^2, \\ \Gamma(\tilde{s} \rightarrow \gamma Z) &= \frac{\alpha G_F^2 m_W^2 (m_{\tilde{s}}^2 - m_Z^2)^3}{64\pi^4 m_{\tilde{s}}^3} \left| \frac{6 - 16s_w^2}{3c_w} s_\xi A_{1/2}^{\gamma Z}(\tilde{\kappa}_t, \mathbf{z}_t) + s_\xi c_w A_1^{\gamma Z}(\tilde{\kappa}_W, \mathbf{z}_W) \right. \\ &\quad \left. - \frac{1 - 2s_w^2}{c_w} \sum_{a=1}^2 \frac{\lambda_{\tilde{s}H_a} v \tilde{v}}{2m_{H_a}^2} A_0^{\gamma Z}(\tilde{\kappa}_{H_a}, \mathbf{z}_{H_a}) \right|^2, \quad (15)\end{aligned}$$

where  $\tilde{\kappa}_\beta = 4m_\beta^2/m_{\tilde{s}}^2$  and in this case we set  $\alpha = 1/125$ .

The aforementioned  $s$  decay channels are the relevant contributions to  $\Gamma_{\tilde{s}}$ . It follows that we can write for the branching fraction of  $\tilde{s} \rightarrow \gamma\gamma$

$$\begin{aligned}\mathcal{B}(\tilde{s} \rightarrow \gamma\gamma) &= \frac{\Gamma_{\tilde{s} \rightarrow \gamma\gamma}}{\Gamma_{\tilde{s}}}, \\ \Gamma_{\tilde{s}} &\simeq \Gamma(\tilde{s} \rightarrow \gamma\gamma) + \Gamma(\tilde{s} \rightarrow \gamma Z) + \Gamma(\tilde{s} \rightarrow hh) + 247 \text{ GeV } s_\xi^2 + \sum_{\text{inert}} \Gamma(\tilde{s} \rightarrow \mathcal{X}\mathcal{Y}), \quad (16)\end{aligned}$$

where in the last term of the second line the sum includes only decay modes with the inert scalar masses satisfying  $m_{\mathcal{X}} + m_{\mathcal{Y}} < m_{\tilde{s}}$ .

## IV. CONSTRAINTS

### A. Theoretical constraints

The parameters in the scalar potential need to meet a number of theoretical requirements. The stability of the vacuum implies that  $\mathcal{V}$  must be bounded from below. This entails that

$$\lambda_1, \lambda_\zeta, \lambda_{21}, \lambda_{22} > 0, \quad \begin{vmatrix} \lambda_1 & \lambda'_1 & \lambda'_2 \\ \lambda'_1 & \lambda_{21} & \lambda'_3 \\ \lambda'_2 & \lambda_6^0 + \lambda_7^0 & \lambda_{22} \end{vmatrix} > 0, \quad \begin{vmatrix} \lambda_1 & \lambda_{3\zeta}^0 & \lambda'_1 & \lambda'_2 \\ \lambda_{3\zeta}^0 & \lambda_x & \lambda_{1\zeta}^0 & \lambda_{2\zeta}^0 \\ \lambda'_1 & \lambda_{1\zeta}^0 & \lambda_{21} & \lambda'_3 \\ \lambda'_2 & \lambda_{2\zeta}^0 & \lambda'_3 & \lambda_{22} \end{vmatrix} > 0, \quad (17)$$

where  $\lambda_x^0 \equiv \text{Min}(0, \lambda_x)$ ,  $\lambda'_1 = \min(0, \lambda_{31} + \lambda_{41})$ ,  $\lambda'_2 = \min(0, \lambda_{32} + \lambda_{42})$ , and  $\lambda'_3 = \min(0, \lambda_6 + \lambda_7)$ . In addition, for the theory to remain perturbative the magnitudes of the  $\lambda$  parameters need to be capped. Thus, in numerical work we impose  $|\lambda_x| < 4\pi$  for the individual couplings, which is similar to the condition in the two-Higgs-doublet case [17].

### B. Electroweak precision tests

The nonstandard interactions in Eq. (8) and those induced by the  $\phi$ - $\zeta$  mixing bring about changes,  $\Delta S$  and  $\Delta T$ , to the so-called oblique electroweak parameters  $S$  and  $T$  which encode the impact of new physics not coupled directly to SM fermions [18]. At the one-loop level [18, 19]

$$\begin{aligned} \frac{\alpha \Delta S}{4c_w^2 s_w^2} &= \frac{A_{ZZ}(m_Z^2) - A_{ZZ}(0)}{m_Z^2} - A'_{\gamma\gamma}(0) - \frac{c_w^2 - s_w^2}{c_w s_w} A'_{\gamma Z}(0), \\ \alpha \Delta T &= \frac{A_{WW}(0)}{m_W^2} - \frac{A_{ZZ}(0)}{m_Z^2}, \end{aligned} \quad (18)$$

where  $A_{XY}(q^2)$  are functions that can be extracted from the vacuum polarization tensors  $\Pi_{XY}^{\mu\nu}(q^2) = A_{XY}(q^2)g^{\mu\nu} + [q^\mu q^\nu \text{ terms}]$  of the SM gauge bosons due to the new scalars' impact at the loop level, and  $A'_{XY}(0) = [dA_{XY}(q^2)/dq^2]_{q^2=0}$ . Here the pertinent loop diagrams are depicted in Fig. 1.

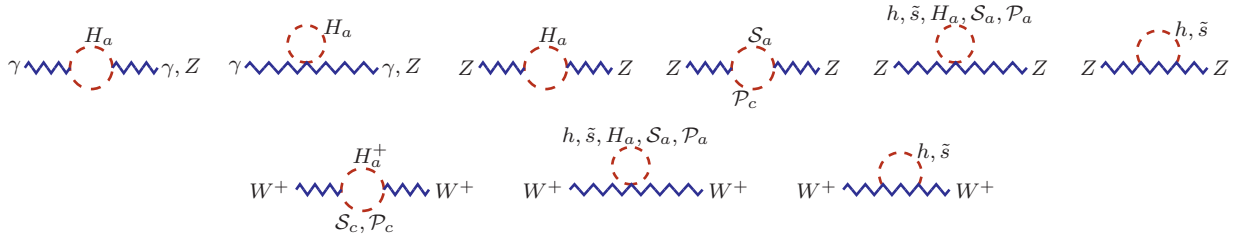


FIG. 1: Feynman diagrams for the contributions of the scalar singlet and inert scalar doublets to the oblique electroweak parameters  $\Delta S$  and  $\Delta T$ .

After evaluating them and subtracting the SM contributions, we arrive at

$$\begin{aligned}
6\pi \Delta S &= \ln \frac{m_{\mathcal{S}_1} m_{\mathcal{S}_2}}{m_{H_1} m_{H_2}} - \frac{5}{6} + \cos^2(\theta_S + \theta_P) \tilde{F}(m_{\mathcal{S}_1}, m_{\mathcal{P}_1}, m_{\mathcal{S}_2}, m_{\mathcal{P}_2}) \\
&+ \sin^2(\theta_S + \theta_P) \tilde{F}(m_{\mathcal{S}_1}, m_{\mathcal{P}_2}, m_{\mathcal{S}_2}, m_{\mathcal{P}_1}) \\
&+ s_\xi^2 \left\{ \frac{m_{\tilde{s}}^2 - m_h^2}{4m_Z^2} + \left[ \frac{11m_Z^2 - m_h^2}{(m_Z^2 - m_h^2)^2} + \frac{1}{m_Z^2} \right] \frac{\mathcal{F}(m_h, m_Z)}{2} \right. \\
&\left. - \left[ \frac{11m_Z^2 - m_{\tilde{s}}^2}{(m_Z^2 - m_{\tilde{s}}^2)^2} + \frac{1}{m_Z^2} \right] \frac{\mathcal{F}(m_{\tilde{s}}, m_Z)}{2} \right\}, \\
16\pi m_W^2 s_w^2 \Delta T &= \cos^2(\theta_H - \theta_S) (\mathcal{F}(m_{H_1}, m_{\mathcal{S}_1}) + \mathcal{F}(m_{H_2}, m_{\mathcal{S}_2})) \\
&+ \sin^2(\theta_H - \theta_S) (\mathcal{F}(m_{H_1}, m_{\mathcal{S}_2}) + \mathcal{F}(m_{H_2}, m_{\mathcal{S}_1})) \\
&+ \cos^2(\theta_H + \theta_P) (\mathcal{F}(m_{H_1}, m_{\mathcal{P}_1}) + \mathcal{F}(m_{H_2}, m_{\mathcal{P}_2})) \\
&+ \sin^2(\theta_H + \theta_P) (\mathcal{F}(m_{H_2}, m_{\mathcal{P}_1}) + \mathcal{F}(m_{H_1}, m_{\mathcal{P}_2})) \\
&- \cos^2(\theta_S + \theta_P) (\mathcal{F}(m_{\mathcal{S}_1}, m_{\mathcal{P}_1}) + \mathcal{F}(m_{\mathcal{S}_2}, m_{\mathcal{P}_2})) \\
&- \sin^2(\theta_S + \theta_P) (\mathcal{F}(m_{\mathcal{S}_1}, m_{\mathcal{P}_2}) + \mathcal{F}(m_{\mathcal{P}_1}, m_{\mathcal{S}_2})) \\
&+ 3s_\xi^2 (\mathcal{F}(m_W, m_h) - \mathcal{F}(m_W, m_{\tilde{s}}) - \mathcal{F}(m_Z, m_h) + \mathcal{F}(m_Z, m_{\tilde{s}})), \quad (19)
\end{aligned}$$

where

$$\mathcal{F}(m, n) = \frac{m^2 + n^2}{2} - \frac{m^2 n^2}{m^2 - n^2} \ln \frac{m^2}{n^2}, \quad (20)$$

$$\begin{aligned}
\tilde{F}(m_1, n_1, m_2, n_2) &= \left[ \frac{m_1^2 + n_1^2}{(m_1^2 - n_1^2)^2} - \frac{1}{m_1^2} \right] \frac{\mathcal{F}(m_1, n_1)}{2} + \left[ \frac{m_2^2 + n_2^2}{(m_2^2 - n_2^2)^2} - \frac{1}{m_2^2} \right] \frac{\mathcal{F}(m_2, n_2)}{2} \\
&+ \frac{n_1^2}{4m_1^2} + \frac{n_2^2}{4m_2^2}, \quad (21)
\end{aligned}$$

and hence  $\mathcal{F}(m, m) = 0$  and  $\tilde{F}(m, m, n, n) = 5/6$ . To check these results, we have also obtained them by employing the formulas provided in Ref. [20]. In our numerical analysis, we apply the  $\Delta S$  and  $\Delta T$  ranges determined in Ref. [19].

### C. Collider constraints

Based on Eq. (8), we may infer from the measured widths of the  $W$  and  $Z$  bosons and the absence yet of evidence for non-SM particles in their decay modes that for  $a, b = 1, 2$

$$m_{H_a} + m_{\mathcal{S}_b} > m_W, \quad m_{H_a} + m_{\mathcal{P}_b} > m_W, \quad 2m_{H_a} > m_Z, \quad m_{\mathcal{S}_a} + m_{\mathcal{P}_b} > m_Z. \quad (22)$$

The null results so far of direct searches for new particles at  $e^+e^-$  colliders also translate into lower limits on these masses, especially those of the charged scalars. In our numerical exploration we will then generally consider the mass regions  $m_{H_a, \mathcal{S}_a, \mathcal{P}_a} > 100 \text{ GeV}$ .

Given that the mixing parameter  $c_\xi$  defined in Eq. (5) is the rescaling factor of the  $h$  couplings to ordinary fermions and weak bosons with respect to their SM counterparts, it needs to satisfy the findings in the LHC experiments that the  $h$  couplings cannot deviate by much more than  $\sim 10\%$  from their SM values [21]. Moreover, for models with a singlet scalar which mixes with the noninert scalar doublet, global fits [22] to the data yield  $|c_\xi| \gtrsim 0.86$ . Consequently, we may place the restraint

$$|s_\xi| < 0.3. \quad (23)$$

Since the decay  $h \rightarrow \gamma\gamma$  has been measured at the LHC, the data imply restrictions on the  $H_{1,2}$  contributions to  $\Gamma(h \rightarrow \gamma\gamma)$ , which we will take into account. On the other hand, although the invisible decay channel of  $h$  is also subject to LHC searches, its limit will not apply to our case because the inert scalar masses are chosen to exceed  $m_h$ .

Additional constraints on our scenario come from the fact that searches for new physics in LHC Run 1 did not produce any clear signals of  $\tilde{s}$  in its possible decay modes. For the major ones, the data from  $pp$  collisions at  $\sqrt{s} = 8$  TeV imply the estimated cross-section limits [5]

$$\begin{aligned} \sigma(pp \rightarrow \tilde{s} \rightarrow \gamma\gamma)_{8\text{ TeV}} &\lesssim 2.3 \text{ fb} [23, 24], \\ \sigma(pp \rightarrow \tilde{s} \rightarrow \gamma Z)_{8\text{ TeV}} &\lesssim 4.0 \text{ fb} [25], \\ \sigma(pp \rightarrow \tilde{s} \rightarrow WW)_{8\text{ TeV}} &\lesssim 47 \text{ fb} [26, 27], \\ \sigma(pp \rightarrow \tilde{s} \rightarrow ZZ)_{8\text{ TeV}} &\lesssim 27 \text{ fb} [28], \\ \sigma(pp \rightarrow \tilde{s} \rightarrow hh)_{8\text{ TeV}} &\lesssim 41 \text{ fb} [29], \\ \sigma(pp \rightarrow \tilde{s} \rightarrow t\bar{t})_{8\text{ TeV}} &\lesssim 700 \text{ fb} [30]. \end{aligned} \quad (24)$$

## V. NUMERICAL RESULTS

Since the  $\tilde{s}$  couplings to SM fermions and weak bosons are  $s_\xi$  times their SM Higgs counterparts, we can estimate the gluon fusion and vector-boson ( $W$  and  $Z$ ) fusion contributions to the cross section  $\sigma(pp \rightarrow \tilde{s})$  from those of a 750 GeV SM Higgs at  $\sqrt{s} = 13$  TeV, namely [31, 32]  $\sigma_{gF}(pp \rightarrow h_{\text{SM}}^{750}) = 4.693 \times 156.8 \text{ fb} \simeq 736 \text{ fb}$  and  $\sigma_{VBF}(pp \rightarrow h_{\text{SM}}^{750}) = 2.496 \times 52.35 \text{ fb} \simeq 131 \text{ fb}$ . Thus

$$\sigma_{gF+VBF}(pp \rightarrow \tilde{s}) = s_\xi^2 \times 867 \text{ fb}. \quad (25)$$

Another contribution to  $\sigma(pp \rightarrow \tilde{s})$  comes from photon fusion [8–10, 33]. It has been considered in other studies on this diphoton excess [11] and can expectedly yield substantial effects if  $\mathcal{B}(\tilde{s} \rightarrow \gamma\gamma)$  is sizable. At  $\sqrt{s} = 13$  TeV, the cross section of this production mode is [10]

$$\sigma_{\gamma F}(pp \rightarrow \tilde{s}) = 1.08 \times 10^4 \times \frac{\Gamma_{\tilde{s}}}{45 \text{ GeV}} \times \mathcal{B}(\tilde{s} \rightarrow \gamma\gamma) \text{ fb}, \quad (26)$$

owing to the elastic, partially inelastic, and fully inelastic collisions of the protons, the latter two being dominant [8, 10]. Therefore, the total production cross-section of  $\tilde{s}$  decaying into the diphoton is

$$\sigma(pp \rightarrow \tilde{s} \rightarrow \gamma\gamma) = [\sigma_{gF+VBF}(pp \rightarrow \tilde{s}) + \sigma_{\gamma F}(pp \rightarrow \tilde{s})] \times \mathcal{B}(\tilde{s} \rightarrow \gamma\gamma), \quad (27)$$

where  $\mathcal{B}(\tilde{s} \rightarrow \gamma\gamma)$  is given by Eq. (16).

Employing Eq. (27), we explore the parameter space of the model in order to attain the cross-section level inferred from the ATLAS and CMS reports on the 750 GeV diphoton excess [1–4], namely [5]

$$\sigma(pp \rightarrow \tilde{s} \rightarrow \gamma\gamma)_{\text{LHC}} \sim (2 - 13) \text{ fb}, \quad (28)$$

as well as the  $\tilde{s}$  total width  $\Gamma_{\tilde{s}} \leq 50 \text{ GeV}$ . Simultaneously, we take into account the perturbativity and vacuum stability conditions, oblique electroweak parameter tests, and restraints from LHC measurements of  $\mathcal{B}(h \rightarrow \gamma\gamma)$ , as discussed in Sec. IV. Furthermore, we consider the charged scalars' mass regions  $m_{H_a}^2 > 100 \text{ GeV}$  and let  $\tilde{v}$ , the VEV of the singlet scalar, vary between 3 and 10 TeV, for  $\tilde{v} < \mathcal{O}(1 \text{ TeV})$  would be inadequate for helping enhance the  $\tilde{s}\gamma\gamma$  coupling to the right magnitude.

As it turns out, there are viable regions in the model parameter space which satisfy the different requirements. To illustrate this, we present in Fig. 2 the distributions of approximately fifteen thousand randomly-generated benchmark points on the planes of various pairs of quantities. The top left panel shows  $\mathcal{R}_{\gamma\gamma}^h = \Gamma(h \rightarrow \gamma\gamma)/\Gamma_0(h \rightarrow \gamma\gamma)$  versus  $\mathcal{R}_{\gamma Z}^h = \Gamma(h \rightarrow \gamma Z)/\Gamma_0(h \rightarrow \gamma Z)$ , where  $\Gamma_0(h \rightarrow \gamma\gamma, \gamma Z)$  stand for the SM rates and are the same in form as  $\Gamma(h \rightarrow \gamma\gamma, \gamma Z)$  in Eq. (14), respectively, but with  $c_\xi = 1$  and  $\lambda_{hH_aH_a} = 0$ . Clearly, the model predicts a positive correlation between  $\mathcal{R}_{\gamma\gamma}^h$  and  $\mathcal{R}_{\gamma Z}^h$ , which will be testable once the empirical information on  $h \rightarrow \gamma Z$  has become precise enough. In view of the red solid (blue dotted) horizontal lines marking the  $1\sigma$  range of  $\mathcal{R}_{\gamma\gamma}^h$  from ATLAS (CMS) [21], we expect that many of the predictions which still agree well with the current data will also be tested by upcoming LHC measurements. In addition, using the color guide on the vertical palette accompanying the plot, we see that the preferred values of the mass  $m_{H_1}$  of the lighter of the charged inert scalars are not far from  $m_{\tilde{s}}/2$ . This is not unexpected because  $H_1$  with a mass near  $m_{\tilde{s}}/2$  helps maximize the  $\tilde{s} \rightarrow \gamma\gamma$  rate.

The top right and middle panels of Fig. 2 exhibit the distributions on the  $m_{H_1}$ - $m_{H_2}$ ,  $m_{S_1}$ - $m_{S_2}$ , and  $m_{P_1}$ - $m_{P_2}$  planes. Evidently, all the inert scalars' masses are greater than  $m_{\tilde{s}}/2$ , but  $m_{H_1}$ , as already mentioned in the last paragraph, and  $m_{S_1}$  do not reach very far away from  $m_{\tilde{s}}/2$ , while  $m_{P_1}$  can go up to 730 GeV or so. In contrast, the values of  $m_{H_2, S_2, P_2}$  lie predominantly in the multi-TeV region, but we also see numerous points corresponding to  $m_{H_2, S_2, P_2}$  around or below 1 TeV. For all these masses, the invisible decay channel of  $\tilde{s}$  into a pair of inert scalars is of course closed. Based on the accompanying palettes, which provide color guides on the mixing parameters  $s_{H,S,P}^2 = \sin^2 \theta_{H,S,P}$ , we deduce that the mixing in each of the three sectors is very suppressed for the majority of the benchmark points, with  $s_{H,S,P}^2 < 10^{-4}$ , whereas for  $m_{H_2, S_2, P_2} \leq \mathcal{O}(1 \text{ TeV})$  the mixing can be significant, with  $|s_{H,S,P}|$  as high as  $\mathcal{O}(0.7)$ . Recalling Eq. (19) for  $\Delta S$  and  $\Delta T$ , one realizes that these different results on the masses and mixing of the inert scalars comply with the restrictions from electroweak precision data.

The bottom left panel of Fig. 2 depicts the maximum size of individual quartic scalar couplings versus the minimum size of them, with the palette reading the cross section  $\sigma(pp \rightarrow \tilde{s} \rightarrow \gamma\gamma)$  in fb. It is obvious that one or more of the couplings need to be fairly large in magnitude, exceeding 6 for most of the benchmarks, which is one of the conditions for the cross section to rise to the desired level. The resulting predictions for  $\sigma(pp \rightarrow \tilde{s} \rightarrow \gamma\gamma)$  appear to lie primarily within the range of 2-7 fb. We also notice that for a preponderance of the points the minimum of the quartic couplings is  $\sim 0.005$  or higher, which happens to belong to  $\lambda_\zeta$ . In these cases,  $m_{\tilde{s}}^2$  is chiefly determined by the  $m_\zeta^2 = \lambda_\zeta \tilde{v}^2$  contribution, as can be concluded from Eq. (5).

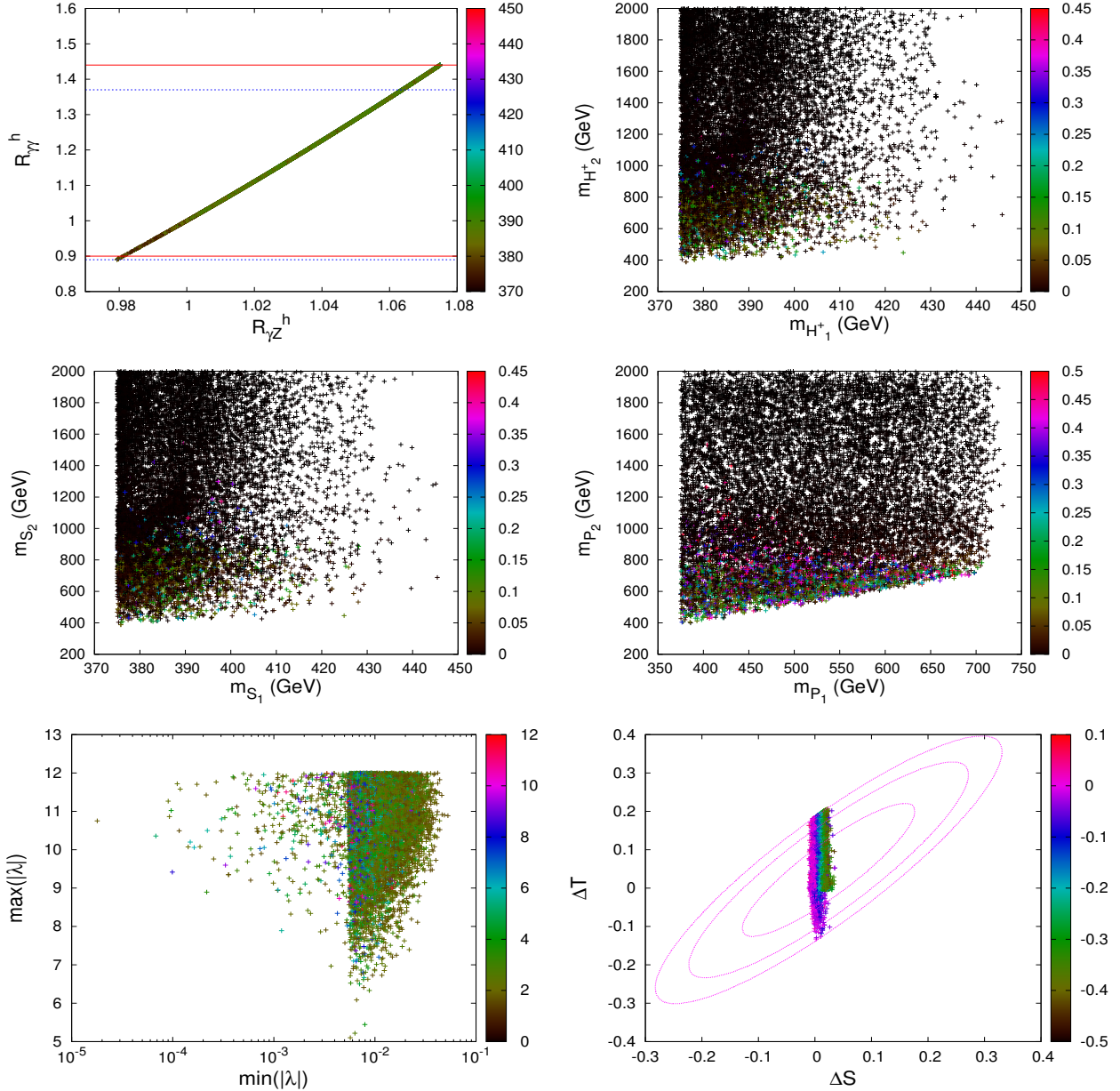


FIG. 2: Top left panel: the ratio  $\mathcal{R}_{\gamma\gamma}^h = \Gamma(h \rightarrow \gamma\gamma)/\Gamma(h \rightarrow \gamma\gamma)_{\text{SM}}$  versus its  $\gamma Z$  counterpart; the horizontal lines mark the  $1\sigma$  ranges of  $\mathcal{R}_{\gamma\gamma}^h$  from ATLAS and CMS [21]; the palette reads the value of  $m_{H_1}$  in GeV. Top right and middle panels: the masses of the inert scalars; the palettes read their respective mixing parameters  $s_{H,S,P}^2 = \sin^2\theta_{H,S,P}$ . Bottom left panel: the maximum and minimum magnitudes of the scalars' quartic couplings  $\lambda$ s; the palette reads the cross section  $\sigma(pp \rightarrow \tilde{s} \rightarrow \gamma\gamma)$  in fb. Bottom right panel: the oblique electroweak precision parameters,  $\Delta S$  and  $\Delta T$ ; the contours, from smallest to biggest, represent the empirical 68%, 95%, and 99% confidence level, respectively; the palette reads the relative mass difference  $1 - (m_{S_1} + m_{P_1})/(2m_{H_1})$ .

The bottom right panel of Fig. 2 displays the new scalars' contributions to the oblique electroweak parameters. The plot shows that a substantial fraction of the benchmarks are within the empirical  $1\sigma$  area. With the palette signifying the amount of relative mass split-

ting  $\hat{\delta} = 1 - (m_{S_1} + m_{P_1})/(2m_{H_1})$  between  $H_1$  and its lightest neutral counterparts, we also observe that  $\Delta S$  has a dependence on  $\hat{\delta}$ , which is similar to the situation in a newly proposed model involving an inert scalar doublet [34].

Before proceeding to the next figure, we would like to remark that the aforesaid tendency of the bulk of  $m_{H_2, S_2, P_2}$  values to be in the multi-TeV region is attributable to the necessity for one or more of the scalar quartic couplings and  $\tilde{v}$  to be big enough to boost the  $\tilde{s} \rightarrow \gamma\gamma$  rate to the desired amount. On the other hand,  $m_{H_1, S_1, P_1}$  have to be fairly close to  $m_{\tilde{s}}/2$  and in numerous cases  $m_{H_2, S_2, P_2}$  can also be sub-TeV, implying that a degree of fine tuning is unavoidable to achieve such relatively low masses. More precisely, this entails partial cancelation of order  $10^{-4}$  or so mainly between the  $\mu_{2a}^2$  and  $\lambda_{a\zeta}\tilde{v}^2$  parts of  $m_{c_{a,n_a}}^2$  in  $m_{H_a, S_a, P_a}$ , as can be inferred from Eqs. (6), (7), (A2), and (A4). We further remark that, as  $m_{H_2, S_2, P_2}$  are large for a good many of the benchmarks, it seems that our scenario may need only one of the inert doublets to explain the 750 GeV diphoton resonance in light of the currently limited experimental information. Nevertheless, given that  $m_{H_2, S_2, P_2}$  with sub-TeV values can also be very well accommodated, if future measurements confirm that  $\tilde{s}$  exists and probe its couplings and other properties in more detail, the acquired data may allow us to ascertain whether the second inert doublet is also necessary.<sup>1</sup> Later collider quests may offer complementary information on the existence of  $\eta_{1,2}$  because of their interactions with SM gauge bosons according to Eq. (8). Due to the inert scalars'  $U(1)_D$  charges, the search channels, such as  $q\bar{q} \rightarrow Z^* \rightarrow S_a S_a, H_a^+ H_a^- Z, P_a P_a Z$ ,  $q\bar{q} \rightarrow \gamma^* \rightarrow H_a^+ H_a^- \gamma$ , and  $\bar{q}q' \rightarrow W^* \rightarrow H_1 S_2$ , each scalar decaying (possibly sequentially) to another and a (real or virtual) SM gauge boson if kinematically allowed, would have the signature of at least one (real or virtual) SM gauge boson plus missing energy.

For a closer view on  $\sigma(pp \rightarrow \tilde{s} \rightarrow \gamma\gamma)$ , we graph benchmarks for it versus the  $\tilde{s}$  total width,  $\Gamma_{\tilde{s}}$ , in the top left panel of Fig. 3. Obviously, our parameter space of interest can yield a cross section within the empirical range in Eq. (28) and also  $\Gamma_{\tilde{s}}$  between  $\sim 1$  and  $6$  GeV. With the palette reading the fractional value of the combined contribution from gluon fusion and vector-boson fusion, it is clear that in these instances the role of photon fusion is crucial, being responsible for between  $\sim 80$  percent and upper-ninety percent of  $\sigma(pp \rightarrow \tilde{s} \rightarrow \gamma\gamma)$ .

Correspondingly, as the top right panel of Fig. 3 reveals, the branching fraction  $\mathcal{B}(\tilde{s} \rightarrow \gamma\gamma)$  varies from about 2 to 22 percent, whereas  $\mathcal{B}(\tilde{s} \rightarrow hh)$  is mostly between 15 and 23 percent. The substantial  $\mathcal{B}(\tilde{s} \rightarrow \gamma\gamma)$  numbers have resulted from the aforementioned big size of one or more of the quartic couplings,  $\tilde{v}$  being in the 3-10 TeV range, and the  $\tilde{s}\gamma\gamma$  coupling dominated by the  $H_a$  loop contribution with  $m_{H_1} \sim m_{\tilde{s}}/2$  for the majority of the benchmarks.

Still with the same panel, from the palette one can see that the favored mixing between the scalar singlet and noninert doublet is rather small, with  $s_\xi^2 \leq \mathcal{O}(0.02)$ , which is expected at least on account of the requirements from electroweak precision data and compatible with results found in very recent literature [7]. Accordingly, one can deduce from Eq. (5), for  $m_\phi < m_\zeta$ , the approximation  $m_{\tilde{s}} \sim \sqrt{\lambda_\zeta}\tilde{v}$ , and for our choice of  $\tilde{v} = 3\text{-}10$  TeV this causes  $\lambda_\zeta$  to be quite

---

<sup>1</sup> It might also be possible to embed this model in a bigger context, such as the scotogenic model recently proposed in [35], where the presence of the inert doublets is essential because they are both needed to generate light Majorana neutrino masses via one-loop interactions with SM-singlet Dirac fermions which include DM candidates. However, in such an expanded scenario, our results would likely be different.

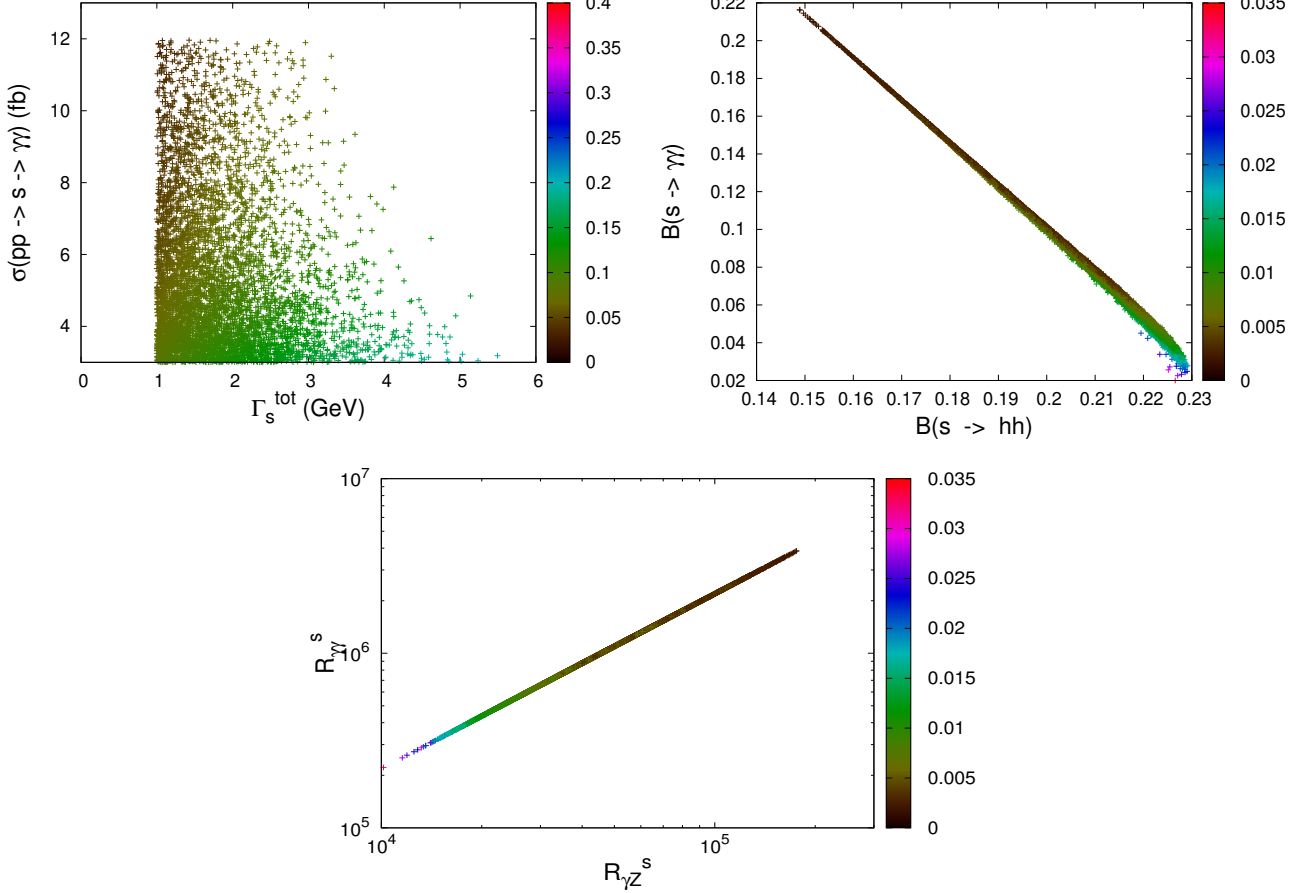


FIG. 3: Top left panel: the cross section  $\sigma(pp \rightarrow \tilde{s} \rightarrow \gamma\gamma)$  versus the total  $\tilde{s}$  width  $\Gamma_{\tilde{s}} = \Gamma_{\tilde{s}}^{\text{tot}}$ ; the palette reads the fractional amount of the combined contribution in Eq. (25) from gluon fusion and vector-boson fusion. Top right panel: the branching fractions  $\mathcal{B}(\tilde{s} \rightarrow \gamma\gamma)$  and  $\mathcal{B}(\tilde{s} \rightarrow hh)$ ; the palette reads  $s_\xi^2 = \sin^2 \xi$ . Bottom panel: the ratios  $\mathcal{R}_{\gamma\gamma}^s$  and  $\mathcal{R}_{\gamma Z}^s$  of  $\Gamma(\tilde{s} \rightarrow \gamma\gamma, \gamma Z)$ , respectively, to their counterparts without the  $H_{1,2}$  contributions; the palette reads  $s_\xi^2$ .

suppressed, below  $\mathcal{O}(0.06)$ . These findings fit the comments earlier concerning the bottom left panel of Fig. 2.

The bottom panel of Fig. 3 depicts some comparison of  $\tilde{s} \rightarrow \gamma\gamma$  and  $\tilde{s} \rightarrow \gamma Z$ , particularly  $\mathcal{R}_{\gamma\gamma}^s = \Gamma(\tilde{s} \rightarrow \gamma\gamma)/\Gamma_0(\tilde{s} \rightarrow \gamma\gamma)$  versus  $\mathcal{R}_{\gamma Z}^s = \Gamma(\tilde{s} \rightarrow \gamma Z)/\Gamma_0(\tilde{s} \rightarrow \gamma Z)$ , with  $\Gamma_0(\tilde{s} \rightarrow \gamma\gamma, \gamma Z)$  being the same in form as  $\Gamma(\tilde{s} \rightarrow \gamma\gamma, \gamma Z)$  in Eq. (15), respectively, but with  $\lambda_{hH_aH_a} = 0$ . The graph reveals that the  $H_{1,2}$  loops can enhance the  $\tilde{s} \rightarrow \gamma\gamma, \gamma Z$  rates by several orders of magnitude relative to the case without  $H_{1,2}$  and that there is a positive correlation between  $\Gamma(\tilde{s} \rightarrow \gamma\gamma, \gamma Z)$ , which can be checked experimentally. In addition, for all the benchmarks our computation yields  $\mathcal{R}_{\gamma\gamma}^s \simeq 22 \mathcal{R}_{\gamma Z}^s$  as well as  $\Gamma(\tilde{s} \rightarrow \gamma\gamma) \simeq 1.3 \Gamma(\tilde{s} \rightarrow \gamma Z)$ . The latter translates into  $\sigma(pp \rightarrow \tilde{s} \rightarrow \gamma\gamma) \simeq 1.3 \sigma(pp \rightarrow \tilde{s} \rightarrow \gamma Z)$  and hence constitutes another signature of the model which may also be checked soon at the LHC, as the prediction for  $\sigma(pp \rightarrow \tilde{s} \rightarrow \gamma Z)$  is roughly an order of magnitude below the upper limits recently reported by ATLAS [36] and CMS [37].

Other signatures may be accessible by probing  $pp \rightarrow \tilde{s} \rightarrow hh, W^+W^-, ZZ, t\bar{t}$ , although their cross sections depend on  $\xi$  and other parameters. Still, given that  $\mathcal{B}(\tilde{s} \rightarrow hh) = \mathcal{O}(0.2)$  as

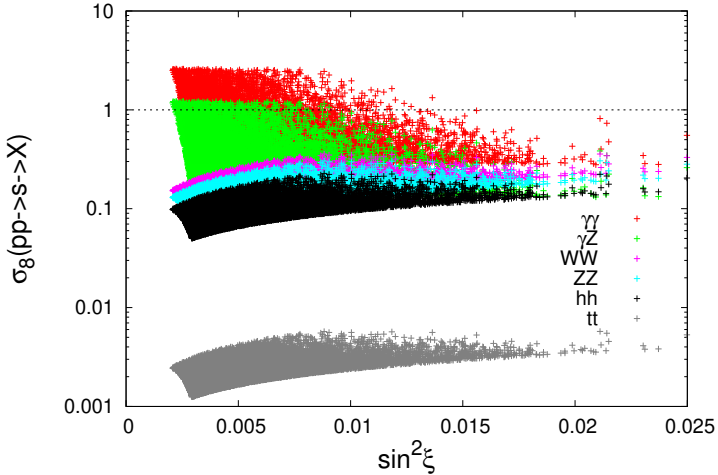


FIG. 4: The cross sections of  $pp \rightarrow \tilde{s} \rightarrow X$  for  $X = \gamma\gamma, \gamma Z, W^+W^-, ZZ, hh, t\bar{t}$  at the center-of-mass energy  $\sqrt{s} = 8$  TeV, each normalized by the corresponding empirical upper-limit from Eq. (24), versus the  $\phi$ - $\varsigma$  mixing parameter  $s_\xi^2$ . Points above the horizontal dotted line are excluded.

indicated above, the  $hh$  channel is potentially reachable if the  $h$  pair can be observed with good precision. Furthermore, since  $\tilde{s} \rightarrow W^+W^-, ZZ, t\bar{t}$  have rates adhering to the ratio in Eq. (12), the cross sections of  $pp \rightarrow \tilde{s} \rightarrow W^+W^-, ZZ, t\bar{t}$  are predicted to obey the same ratio. Therefore, if  $|s_\xi| = \mathcal{O}(0.1)$ , they may be sufficiently measurable to allow us to test these predictions.

Now, analogously to Eq. (27), at  $\sqrt{s} = 8$  TeV the cross section of  $pp \rightarrow \tilde{s}$  is

$$\sigma(pp \rightarrow \tilde{s})_{8 \text{ TeV}} = \sigma_{gF+VBF}(pp \rightarrow \tilde{s})_{8 \text{ TeV}} + \sigma_{\gamma F}(pp \rightarrow \tilde{s})_{8 \text{ TeV}} \quad (29)$$

consisting of the gluon-, vector-boson-, and photon-fusion contributions [10, 31]

$$\begin{aligned} \sigma_{gF+VBF}(pp \rightarrow \tilde{s})_{8 \text{ TeV}} &= s_\xi^2 \times (156.8 + 52.35) \text{ fb}, \\ \sigma_{\gamma F}(pp \rightarrow \tilde{s})_{8 \text{ TeV}} &= 5.5 \times 10^3 \times \frac{\Gamma_{\tilde{s}}}{45 \text{ GeV}} \times \mathcal{B}(\tilde{s} \rightarrow \gamma\gamma) \text{ fb}. \end{aligned} \quad (30)$$

Using these, we can evaluate  $\sigma_8(pp \rightarrow \tilde{s} \rightarrow X) \equiv \sigma(pp \rightarrow \tilde{s})_{8 \text{ TeV}} \mathcal{B}(\tilde{s} \rightarrow X)$  in relation to  $s_\xi^2$  for  $X = \gamma\gamma, \gamma Z, W^+W^-, ZZ, hh, t\bar{t}$  divided by the corresponding experimental limits in Eq. (24). We display the results in Fig. 4. It is evident from this plot that these restraints lead to a significant decrease in the number of viable points, as a high percentage of the  $\gamma\gamma$  benchmarks (in red) resides above the horizontal dotted line. However, currently there is considerable uncertainty in the ratio between the 8 TeV and 13 TeV estimates of the photon-fusion contributions, which could imply a reduction of the first numerical factor in  $\sigma_{\gamma F}(pp \rightarrow \tilde{s})_{8 \text{ TeV}}$  in Eq. (30) by up to twice or more [8–10]. As a consequence, a substantial portion of the parameter space represented by our scan points may evade the no-signal constraints from the Run 1 searches.

## VI. CONCLUSIONS

In this work we have considered the possibility that the observed diphoton excess at an invariant mass of about 750 GeV recently reported by the ATLAS and CMS Collaborations

is an indication of a new spinless particle. To explain it, we propose an extension of the SM with a new sector comprising two inert scalar doublets,  $\eta_{1,2}$ , and a scalar singlet,  $\zeta$ , which transform under a dark Abelian gauge symmetry,  $U(1)_D$ . We identify  $\tilde{s}$ , the heavier one of the mass eigenstates from the mixing of the singlet with the noninert doublet, as the 750 GeV resonance. The inert doublets play an indispensable role because their charged components  $H_{1,2}^\pm$  can give rise to the loop-induced  $\tilde{s}\gamma\gamma$  coupling of the right strength, with suitable choices of the model parameters and without the inclusion of extra colored fermions or bosons. After taking into account the perturbativity condition, the vacuum stability bound, and the constraints from electroweak precision tests, we show that within the allowed parameter space the production cross-section  $\sigma(pp \rightarrow \tilde{s} \rightarrow \gamma\gamma)$  can be of order a few fb, mainly due to the sizable contribution from photon fusion in our scenario, while the total width  $\Gamma_{\tilde{s}}$  lies in the range of 1-6 GeV. The upcoming data from the LHC with improved precision can be expected to test this prediction for  $\Gamma_{\tilde{s}}$ . Lastly, we point out that the model also predicts roughly similar cross-sections of  $pp \rightarrow \tilde{s} \rightarrow \gamma\gamma, \gamma Z$  and a specific ratio involving the cross-sections of  $pp \rightarrow \tilde{s} \rightarrow W^+W^-, ZZ, t\bar{t}$ , all of which may be experimentally verified in the near future.

### Acknowledgments

A.A. is supported by the Algerian Ministry of Higher Education and Scientific Research under the CNEPRU Project No. D01720130042. He would like to thank Xiao-Gang He and J.T. for the warm hospitality at NTU-CTS, where this work was initiated. The work of G.F. was supported in part by the research grant NTU-ERP-102R7701. The work of J.T. was supported in part by the MOE Academic Excellence Program (Grant No. 102R891505). We gratefully acknowledge partial support from the National Center for Theoretical Sciences of Taiwan.

### Appendix A: Scalar masses and couplings

In Eq. (4), the squared-mass matrices  $M_{\phi\zeta,C,0}^2$  and column matrix  $\eta_0$  are given by

$$M_{\phi\zeta}^2 = \begin{pmatrix} m_\phi^2 & \frac{m_{\phi\zeta}^2}{2} \\ \frac{m_{\phi\zeta}^2}{2} & m_\zeta^2 \end{pmatrix}, \quad m_\phi^2 = \lambda_1 v^2, \quad m_\zeta^2 = \lambda_\zeta \tilde{v}^2, \quad m_{\phi\zeta}^2 = 2\lambda_{3\zeta} v\tilde{v}, \quad (\text{A1})$$

$$M_C^2 = \begin{pmatrix} m_{c_1}^2 & \frac{m_{c\zeta}^2}{2} \\ \frac{m_{c\zeta}^{2*}}{2} & m_{c_2}^2 \end{pmatrix}, \quad m_{c_a}^2 = \mu_{2a}^2 + \frac{\lambda_{3a} v^2 + \lambda_{a\zeta} \tilde{v}^2}{2}, \quad m_{c\zeta}^2 = \sqrt{2} \mu_{\eta\zeta} \tilde{v}, \quad (\text{A2})$$

$$M_0^2 = \begin{pmatrix} m_{n_1}^2 & \frac{m_{n\zeta}^2}{2} & 0 & \frac{-\text{Im } m_{c\zeta}^2}{2} \\ \frac{m_{n\zeta}^2}{2} & m_{n_2}^2 & \frac{\text{Im } m_{c\zeta}^2}{2} & 0 \\ 0 & \frac{\text{Im } m_{c\zeta}^2}{2} & m_{n_1}^2 & -\frac{\tilde{m}_{n\zeta}^2}{2} \\ \frac{-\text{Im } m_{c\zeta}^2}{2} & 0 & -\frac{\tilde{m}_{n\zeta}^2}{2} & m_{n_2}^2 \end{pmatrix}, \quad \eta_0 = \begin{pmatrix} \text{Re } \eta_1^0 \\ \text{Re } \eta_2^0 \\ \text{Im } \eta_1^0 \\ \text{Im } \eta_2^0 \end{pmatrix}, \quad (\text{A3})$$

$$\begin{aligned}
m_{n_a}^2 &= \mu_{2a}^2 + \frac{(\lambda_{3a} + \lambda_{4a})v^2 + \lambda_{a\zeta}\tilde{v}^2}{2} = m_{c_a}^2 + \frac{\lambda_{4a}v^2}{2}, \\
m_{n\zeta}^2 &= \frac{\lambda_5}{2}v^2 + \text{Re } m_{c\zeta}^2, \quad \tilde{m}_{n\zeta}^2 = \frac{\lambda_5}{2}v^2 - \text{Re } m_{c\zeta}^2.
\end{aligned} \tag{A4}$$

The constants  $\mu_{2a}^2$  enter only these mass formulas of the inert scalars and can be positive or negative if nonzero. To arrive at  $M_{\phi\zeta}^2$  in Eq. (A1), we have used the relations

$$\mu_1^2 = \frac{-\lambda_1 v^2 - \lambda_{3\zeta}\tilde{v}^2}{2}, \quad \mu_\zeta^2 = \frac{-\lambda_\zeta\tilde{v}^2 - \lambda_{3\zeta}v^2}{2},$$

corresponding to the vanishing of the first derivatives of the potential  $\mathcal{V}$  with respect to  $\phi$  and  $\zeta$ .

If the parameter  $\mu_{\eta\zeta}$  in the potential is complex, so is  $M_{\mathcal{C}}^2$ , which can then be diagonalized with the unitary matrix  $\mathcal{U}_{\mathcal{C}}$  according to

$$\begin{aligned}
\mathcal{U}_{\mathcal{C}} &= \begin{pmatrix} \mathcal{C}_{11} & \mathcal{C}_{12} \\ \mathcal{C}_{21} & \mathcal{C}_{22} \end{pmatrix}, \quad \mathcal{U}_{\mathcal{C}}^\dagger M_{\mathcal{C}}^2 \mathcal{U}_{\mathcal{C}} = \text{diag}(m_{H_1}^2, m_{H_2}^2), \\
\mathcal{C}_{11} &= \frac{+\mu_{\eta\zeta}}{\sqrt{2}|\mu_{\eta\zeta}|} \sqrt{1 + \frac{m_{c_2}^2 - m_{c_1}^2}{m_{H_2}^2 - m_{H_1}^2}} = \frac{\mu_{\eta\zeta}}{|\mu_{\eta\zeta}|} \mathcal{C}_{22}, \\
\mathcal{C}_{12} &= \frac{\mu_{\eta\zeta}}{\sqrt{2}|\mu_{\eta\zeta}|} \sqrt{1 + \frac{m_{c_1}^2 - m_{c_2}^2}{m_{H_2}^2 - m_{H_1}^2}} = \frac{-\mu_{\eta\zeta}}{|\mu_{\eta\zeta}|} \mathcal{C}_{21}.
\end{aligned} \tag{A5}$$

As noted earlier, without loss of generality, we can select  $\mu_{\eta\zeta}$  to be real, rendering  $m_{c\zeta}^2$  real as well, in which case  $\mathcal{U}_{\mathcal{C}}$  has the orthogonal form in Eq. (6).

If  $\mu_{\eta\zeta}$  is complex, the matrix  $\mathcal{O}_0$  that diagonalizes  $M_0^2$  has the form

$$\mathcal{O}_0 = \begin{pmatrix} \mathcal{N}_{11} & \mathcal{N}_{12} & \mathcal{N}_{13} & \mathcal{N}_{14} \\ \mathcal{N}_{21} & \mathcal{N}_{22} & \mathcal{N}_{23} & \mathcal{N}_{24} \\ \mathcal{N}_{31} & \mathcal{N}_{32} & \mathcal{N}_{33} & \mathcal{N}_{34} \\ \mathcal{N}_{41} & \mathcal{N}_{42} & \mathcal{N}_{43} & \mathcal{N}_{44} \end{pmatrix}, \tag{A6}$$

where  $\mathcal{N}_{rs}$  are mostly complicated. With  $\mu_{\eta\zeta}$  being real instead, these elements are much simpler

$$\begin{aligned}
\mathcal{N}_{11} &= \frac{\sigma_{11} \text{sgn}(m_{n\zeta}^2)}{\sqrt{2}} \sqrt{1 + \frac{m_{n_2}^2 - m_{n_1}^2}{m_{\mathcal{S}_2}^2 - m_{\mathcal{S}_1}^2}}, & \mathcal{N}_{12} &= \frac{\sigma_{12}}{\sqrt{2}} \sqrt{1 + \frac{m_{n_1}^2 - m_{n_2}^2}{m_{\mathcal{S}_2}^2 - m_{\mathcal{S}_1}^2}}, \\
\mathcal{N}_{33} &= \frac{\sigma_{33} \text{sgn}(\tilde{m}_{n\zeta}^2)}{\sqrt{2}} \sqrt{1 + \frac{m_{n_2}^2 - m_{n_1}^2}{m_{\mathcal{P}_2}^2 - m_{\mathcal{P}_1}^2}}, & \mathcal{N}_{34} &= \frac{\sigma_{34}}{\sqrt{2}} \sqrt{1 + \frac{m_{n_1}^2 - m_{n_2}^2}{m_{\mathcal{P}_2}^2 - m_{\mathcal{P}_1}^2}}, \\
\mathcal{N}_{22} &= \sigma_{11}\sigma_{12}\mathcal{N}_{11}, \quad \mathcal{N}_{21} = -\sigma_{11}\sigma_{12}\mathcal{N}_{12}, \quad \mathcal{N}_{44} = -\sigma_{33}\sigma_{34}\mathcal{N}_{33}, \quad \mathcal{N}_{43} = \sigma_{33}\sigma_{34}\mathcal{N}_{34}, \\
\mathcal{N}_{13} &= \mathcal{N}_{14} = \mathcal{N}_{23} = \mathcal{N}_{24} = \mathcal{N}_{31} = \mathcal{N}_{32} = \mathcal{N}_{41} = \mathcal{N}_{42} = 0, \\
\sigma_{11}^2 &= \sigma_{12}^2 = 1, \quad \sigma_{33}^2 = \sigma_{34}^2 = 1,
\end{aligned} \tag{A7}$$

where  $\sigma_{11,12,33,34}$  are independent of each other and can each be either  $+1$  or  $-1$ , implying that we can choose  $\sigma_{11}\sigma_{12} = \sigma_{33}\sigma_{34} = +1$  to get the form of  $\mathcal{O}_0$  in Eq. (7).

The  $\lambda$ 's in Eq. (10) are

$$\begin{aligned}\lambda_{hH_1H_1} &= c_\xi (c_H^2 \lambda_{31} + s_H^2 \lambda_{32}) - s_\xi \left[ (c_H^2 \lambda_{1\zeta} + s_H^2 \lambda_{2\zeta}) \frac{\tilde{v}}{v} - \sqrt{2} c_H s_H \frac{\mu_{\eta\zeta}}{v} \right], \\ \lambda_{hH_2H_2} &= c_\xi (c_H^2 \lambda_{32} + s_H^2 \lambda_{31}) - s_\xi \left[ (c_H^2 \lambda_{2\zeta} + s_H^2 \lambda_{1\zeta}) \frac{\tilde{v}}{v} + \sqrt{2} c_H s_H \frac{\mu_{\eta\zeta}}{v} \right],\end{aligned}\quad (\text{A8})$$

$$\lambda_{\tilde{s}hh} = c_\xi [(1 - 3s_\xi^2) \lambda_{3\zeta} + 3s_\xi^2 \lambda_\zeta] + s_\xi [(1 - 3c_\xi^2) \lambda_{3\zeta} + 3c_\xi^2 \lambda_1] \frac{v}{\tilde{v}}, \quad (\text{A9})$$

$$\begin{aligned}\lambda_{\tilde{s}H_1H_1} &= c_\xi \left( c_H^2 \lambda_{1\zeta} + s_H^2 \lambda_{2\zeta} - \sqrt{2} c_H s_H \frac{\mu_{\eta\zeta}}{\tilde{v}} \right) + s_\xi (c_H^2 \lambda_{31} + s_H^2 \lambda_{32}) \frac{v}{\tilde{v}}, \\ \lambda_{\tilde{s}H_2H_2} &= c_\xi \left( c_H^2 \lambda_{2\zeta} + s_H^2 \lambda_{1\zeta} + \sqrt{2} c_H s_H \frac{\mu_{\eta\zeta}}{\tilde{v}} \right) + s_\xi (c_H^2 \lambda_{32} + s_H^2 \lambda_{31}) \frac{v}{\tilde{v}},\end{aligned}\quad (\text{A10})$$

$$\begin{aligned}\lambda_{\tilde{s}\mathcal{S}_1\mathcal{S}_1} &= c_\xi \left( c_S^2 \lambda_{1\zeta} + s_S^2 \lambda_{2\zeta} - \sqrt{2} c_S s_S \frac{\mu_{\eta\zeta}}{\tilde{v}} \right) \\ &\quad + s_\xi [c_S^2 (\lambda_{31} + \lambda_{41}) + s_S^2 (\lambda_{32} + \lambda_{42}) - c_S s_S \lambda_5] \frac{v}{\tilde{v}}, \\ \lambda_{\tilde{s}\mathcal{S}_2\mathcal{S}_2} &= c_\xi \left( c_S^2 \lambda_{2\zeta} + s_S^2 \lambda_{1\zeta} + \sqrt{2} c_S s_S \frac{\mu_{\eta\zeta}}{\tilde{v}} \right) \\ &\quad + s_\xi [c_S^2 (\lambda_{32} + \lambda_{42}) + s_S^2 (\lambda_{31} + \lambda_{41}) + c_S s_S \lambda_5] \frac{v}{\tilde{v}}, \\ \lambda_{\tilde{s}\mathcal{S}_1\mathcal{S}_2} &= c_\xi \left[ c_S s_S (\lambda_{1\zeta} - \lambda_{2\zeta}) + (c_S^2 - s_S^2) \frac{\mu_{\eta\zeta}}{\sqrt{2} \tilde{v}} \right] \\ &\quad + s_\xi [c_S s_S (\lambda_{31} + \lambda_{41} - \lambda_{32} - \lambda_{42}) + \frac{1}{2} (c_S^2 - s_S^2) \lambda_5] \frac{v}{\tilde{v}},\end{aligned}\quad (\text{A11})$$

$$\begin{aligned}\lambda_{\tilde{s}\mathcal{P}_1\mathcal{P}_1} &= c_\xi \left( c_P^2 \lambda_{1\zeta} + s_P^2 \lambda_{2\zeta} + \sqrt{2} c_P s_P \frac{\mu_{\eta\zeta}}{\tilde{v}} \right) \\ &\quad + s_\xi [c_P^2 (\lambda_{31} + \lambda_{41}) + s_P^2 (\lambda_{32} + \lambda_{42}) - c_P s_P \lambda_5] \frac{v}{\tilde{v}}, \\ \lambda_{\tilde{s}\mathcal{P}_2\mathcal{P}_2} &= c_\xi \left( c_P^2 \lambda_{2\zeta} + s_P^2 \lambda_{1\zeta} - \sqrt{2} c_P s_P \frac{\mu_{\eta\zeta}}{\tilde{v}} \right) \\ &\quad + s_\xi [c_P^2 (\lambda_{32} + \lambda_{42}) + s_P^2 (\lambda_{31} + \lambda_{41}) + c_P s_P \lambda_5] \frac{v}{\tilde{v}}, \\ \lambda_{\tilde{s}\mathcal{P}_1\mathcal{P}_2} &= c_\xi \left[ c_P s_P (\lambda_{1\zeta} - \lambda_{2\zeta}) - (c_P^2 - s_P^2) \frac{\mu_{\eta\zeta}}{\sqrt{2} \tilde{v}} \right] \\ &\quad + s_\xi [c_P s_P (\lambda_{31} + \lambda_{41} - \lambda_{32} - \lambda_{42}) + \frac{1}{2} (c_P^2 - s_P^2) \lambda_5] \frac{v}{\tilde{v}}.\end{aligned}\quad (\text{A12})$$

We then find

$$\begin{aligned}\lambda_{hH_1H_1} + \lambda_{hH_2H_2} &= c_\xi (\lambda_{31} + \lambda_{32}) - s_\xi (\lambda_{1\zeta} + \lambda_{2\zeta}) \frac{\tilde{v}}{v}, \\ \lambda_{\tilde{s}H_1H_1} + \lambda_{\tilde{s}H_2H_2} &= c_\xi (\lambda_{1\zeta} + \lambda_{2\zeta}) + s_\xi (\lambda_{31} + \lambda_{32}) \frac{v}{\tilde{v}}.\end{aligned}\quad (\text{A13})$$

- [2] CMS Collaboration, CMS-PAS-EXO-15-004.
- [3] M. Aaboud *et al.* [ATLAS Collaboration], arXiv:1606.03833 [hep-ex].
- [4] V. Khachatryan *et al.* [CMS Collaboration], arXiv:1606.04093 [hep-ex].
- [5] M. Backovic *et al.*, arXiv:1512.04917; S. Knapen *et al.*, arXiv:1512.04928; D. Buttazzo *et al.*, arXiv:1512.04929; R. Franceschini *et al.*, arXiv:1512.04933; S. Di Chiara *et al.*, arXiv:1512.04939; J. Ellis *et al.*, arXiv:1512.05327; M. Low *et al.*, arXiv:1512.05328; A. Kobakhidze *et al.*, arXiv:1512.05585; A. Ahmed *et al.*, arXiv:1512.05771; W. Altmannshofer *et al.*, arXiv:1512.07616.
- [6] S. Sun, arXiv:1411.0131; A. Biswas and A. Lahiri, arXiv:1511.07159; K. Harigaya and Y. Nomura, Phys. Lett. B **754**, 151 (2016) [arXiv:1512.04850]; Y. Mambrini *et al.*, arXiv:1512.04913; A. Angelescu *et al.*, arXiv:1512.04921; Y. Nakai *et al.*, arXiv:1512.04924; A. Pilaftsis, Phys. Rev. D **93**, no. 1, 015017 (2016) [arXiv:1512.04931]; B. Bellazzini *et al.*, arXiv:1512.05330; R.S. Gupta *et al.*, arXiv:1512.05332; E. Molinaro *et al.*, arXiv:1512.05334; S.D. McDermott *et al.*, arXiv:1512.05326; C. Petersson and R. Torre, arXiv:1512.05333; B. Dutta *et al.*, arXiv:1512.05439; P. Cox *et al.*, arXiv:1512.05618; A. Ahmed *et al.*, arXiv:1512.05771; P. Agrawal *et al.*, arXiv:1512.05775; D. Becirevic *et al.*, arXiv:1512.05623; J.M. No *et al.*, arXiv:1512.05700; S.V. Demidov and D.S. Gorbunov, arXiv:1512.05723; W. Chao *et al.*, arXiv:1512.05738; D. Curtin and C.B. Verhaaren, arXiv:1512.05753; L. Bian *et al.*, arXiv:1512.05759; J. Chakrabortty *et al.*, arXiv:1512.05767; D. Aloni *et al.*, arXiv:1512.05778; Y. Bai *et al.*, arXiv:1512.05779; S. Ghosh *et al.*, arXiv:1512.05786; E. Gabrielli *et al.*, Phys. Lett. B **756**, 36 (2016) [arXiv:1512.05961]; J.S. Kim *et al.*, arXiv:1512.06083; A. Alves *et al.*, arXiv:1512.06091; E. Megias *et al.*, arXiv:1512.06106; J. Bernon and C. Smith, arXiv:1512.06113; W. Chao, arXiv:1512.06297; A. Ringwald and K. Saikawa, arXiv:1512.06436; M.T. Arun and P. Saha, arXiv:1512.06335; C. Han *et al.*, arXiv:1512.06376; S. Chang, arXiv:1512.06426; X.F. Han and L. Wang, Phys. Rev. D **93**, no. 5, 055027 (2016) [arXiv:1512.06587]; H. Han *et al.*, arXiv:1512.06562; M.x. Luo *et al.*, arXiv:1512.06670; J. Chang *et al.*, arXiv:1512.06671; D. Bardhan *et al.*, arXiv:1512.06674; T.F. Feng *et al.*, arXiv:1512.06696; M. Dhuria and G. Goswami, arXiv:1512.06782; W.S. Cho *et al.*, arXiv:1512.06824; D. Barducci *et al.*, arXiv:1512.06842; M. Chala *et al.*, Phys. Lett. B **755**, 145 (2016) [arXiv:1512.06833]; I. Chakraborty and A. Kundu, arXiv:1512.06508; R. Ding *et al.*, arXiv:1512.06560; H. Hatanaka, arXiv:1512.06595; O. Antipin *et al.*, arXiv:1512.06708; F. Wang *et al.*, arXiv:1512.06715; J. Cao *et al.*, arXiv:1512.06728; F.P. Huang *et al.*, arXiv:1512.06732; X.J. Bi *et al.*, arXiv:1512.06787; J.S. Kim *et al.*, arXiv:1512.06797; J.M. Cline and Z. Liu, arXiv:1512.06827; K. Kulkarni, arXiv:1512.06836; S.M. Boucenna *et al.*, arXiv:1512.06878; P.S.B. Dev and D. Teresi, arXiv:1512.07243; J. de Blas *et al.*, arXiv:1512.07229; C.W. Murphy, arXiv:1512.06976; A.E.C. Hernandez and I. Nisandzic, arXiv:1512.07165; U.K. Dey *et al.*, arXiv:1512.07212; G.M. Pelaggi *et al.*, arXiv:1512.07225; Q.H. Cao *et al.*, arXiv:1512.07541; J. Gu and Z. Liu, arXiv:1512.07624; W.C. Huang *et al.*, arXiv:1512.07268; M. Chabab *et al.*, arXiv:1512.07280; S. Moretti and K. Yagyu, arXiv:1512.07462; K.M. Patel and P. Sharma, arXiv:1512.07468; M. Badziak, arXiv:1512.07497; S. Chakraborty *et al.*, arXiv:1512.07527; M. Cvetic *et al.*, arXiv:1512.07622; B.C. Allanach *et al.*, arXiv:1512.07645; K. Das and S.K. Rai, arXiv:1512.07789; H. Davoudiasl and C. Zhang, arXiv:1512.07672; J. Liu *et al.*, arXiv:1512.07885; J. Zhang and S. Zhou, arXiv:1512.07889; L.J. Hall *et al.*, arXiv:1512.07904; H. Han *et al.*, arXiv:1512.07992; J.C. Park and S.C. Park, arXiv:1512.08117; D. Chway *et al.*, arXiv:1512.08221; H. An *et al.*, arXiv:1512.08378; F. Wang *et al.*, arXiv:1512.08434; Q.H. Cao *et al.*, arXiv:1512.08441; J. Gao *et al.*, arXiv:1512.08478; P.S.B. Dev *et al.*, JHEP02, 186 (2016) [arXiv:1512.08507]; L. Del Debbio *et al.*, arXiv:1512.08242; A. Salvio and A. Mazumdar, Phys. Lett. B **755**, 469 (2016) [arXiv:1512.08184]; G. Li *et al.*, arXiv:1512.08255; M. Son and A. Urbano, arXiv:1512.08307; Y.L. Tang and S.h. Zhu, arXiv:1512.08323; J. Cao *et*

*al.*, arXiv:1512.08392; C. Cai *et al.*, arXiv:1512.08440; J.E. Kim, Phys. Lett. B **755**, 190 (2016) [arXiv:1512.08467]; W. Chao, arXiv:1512.08484; X.J. Bi *et al.*, arXiv:1512.08497; L.A. Anchordoqui *et al.*, Phys. Lett. B **755**, 312 (2016) [arXiv:1512.08502]; N. Bizot *et al.*, arXiv:1512.08508; Y. Hamada *et al.*, arXiv:1512.08984; A. Pich, Acta Phys. Polon. B **47**, 151 (2016) [arXiv:1512.08749]; L.E. Ibanez and V. Martin-Lozano, arXiv:1512.08777; C.W. Chiang *et al.*, arXiv:1512.08895; S.K. Kang and J. Song, arXiv:1512.08963; S. Kanemura *et al.*, arXiv:1512.09048; S. Kanemura *et al.*, arXiv:1512.09053; P.V. Dong and N.T.K. Ngan, arXiv:1512.09073; I. Low and J. Lykken, arXiv:1512.09089; A.E.C. Hernandez, arXiv:1512.09092; Y. Jiang *et al.*, arXiv:1512.09127; K. Kaneta *et al.*, arXiv:1512.09129; L. Marzola *et al.*, JHEP **1603**, 190 (2016) [arXiv:1512.09136]; E. Ma, arXiv:1512.09159; arXiv:1601.01400; A. Dasgupta *et al.*, arXiv:1512.09202; S. Jung *et al.*, arXiv:1601.00006; X.F. Han *et al.*, Phys. Lett. B **756**, 309 (2016) [arXiv:1601.00534]; P. Ko *et al.*, arXiv:1601.00586; C.T. Potter, arXiv:1601.00240; E. Palti, arXiv:1601.00285; H.J. Kang and W. Wang, arXiv:1601.00373; K. Ghorbani and H. Ghorbani, arXiv:1601.00602; U. Danielsson *et al.*, arXiv:1601.00624; W. Chao, arXiv:1601.00633; T. Modak *et al.*, arXiv:1601.00836; B. Dutta *et al.*, arXiv:1601.00866; A.E.C. Hernandez *et al.*, arXiv:1601.00661; H. Ito *et al.*, arXiv:1601.01144; H. Zhang, arXiv:1601.01355; A. Berlin, arXiv:1601.01381; S. Bhattacharya *et al.*, arXiv:1601.01569; D. Borah *et al.*, arXiv:1601.01828; N. Sonmez, arXiv:1601.01837; L.G. Xia, arXiv:1601.02454; P. Ko and T. Nomura, arXiv:1601.02490; J. Cao *et al.*, arXiv:1601.02570; M.T. Arun and D. Choudhury, arXiv:1601.02321; C. Hati, arXiv:1601.02457; J.H. Yu, arXiv:1601.02609; R. Ding *et al.*, arXiv:1601.02714; Z. Fodor *et al.*, arXiv:1601.03302; J.H. Davis *et al.*, arXiv:1601.03153; L.V. Laperashvili *et al.*, Int. J. Mod. Phys. A **31**, 1650029 (2016) [arXiv:1601.03231]; I. Dorsner *et al.*, arXiv:1601.03267; A. Djouadi *et al.*, arXiv:1601.03696; A.E. Faraggi and J. Rizos, arXiv:1601.03604; L.A. Harland-Lang *et al.*, arXiv:1601.03772; T. Appelquist *et al.*, arXiv:1601.04027; D. Bardhan *et al.*, arXiv:1601.04165; A. Ghoshal, arXiv:1601.04291; T. Nomura and H. Okada, arXiv:1601.04516; W. Chao, arXiv:1601.04678; M.R. Buckley, arXiv:1601.04751; X.F. Han *et al.*, Phys. Lett. B **757**, 537 (2016) [arXiv:1601.04954]; H. Okada and K. Yagyu, arXiv:1601.05038; D.B. Franzosi and M.T. Frandsen, arXiv:1601.05357; A. Martini *et al.*, arXiv:1601.05729; C.W. Chiang and A.L. Kuo, arXiv:1601.06394; U. Aydemir and T. Mandal, arXiv:1601.06761; V. Branchina *et al.*, arXiv:1601.06963; J. Kawamura and Y. Omura, arXiv:1601.07396; M.J. Dolan *et al.*, arXiv:1601.07208; B.J. Kavanagh, arXiv:1601.07330; C.Q. Geng and D. Huang, arXiv:1601.07385; E. Bertuzzo *et al.*, arXiv:1601.07508; I. Ben-Dayan and R. Brustein, arXiv:1601.07564; T. Robens and T. Stefaniak, arXiv:1601.07880; F. del Aguila *et al.*, arXiv:1602.00126; L. Aparicio *et al.*, arXiv:1602.00949; R. Ding *et al.*, arXiv:1602.00977; K. Harigaya and Y. Nomura, arXiv:1602.01092; T. Li *et al.*, arXiv:1602.01377; A. Salvio *et al.*, arXiv:1602.01460; S.F. Ge *et al.*, arXiv:1602.01801; S.I. Godunov *et al.*, arXiv:1602.02380; S.B. Giddings and H. Zhang, arXiv:1602.02793; U.K. Dey and T. Jha, arXiv:1602.03286; U. Ellwanger and C. Hugonie, arXiv:1602.03344; K. J. Bae *et al.*, arXiv:1602.03653; C. Arbelaez *et al.*, arXiv:1602.03607; C. Han *et al.*, arXiv:1602.04204; Y. Hamada *et al.*, arXiv:1602.04170; B. Dasgupta *et al.*, arXiv:1602.04692; C. Delaunay and Y. Soreq, arXiv:1602.04838; Y.J. Zhang *et al.*, arXiv:1602.05539; P.S.B. Dev *et al.*, arXiv:1602.05947; F. Staub *et al.*, arXiv:1602.05581; S. Baek and J.h. Park, arXiv:1602.05588; M. Cvetic *et al.*, arXiv:1602.06257; A. Kobakhidze, arXiv:1602.06363; S. De Curtis *et al.*, arXiv:1602.06437; D.K. Hong and D.H. Kim, arXiv:1602.06628; C. Quigg, arXiv:1602.07020; M. Redi *et al.*, arXiv:1602.07297; D.N. Dinh *et al.*, arXiv:1602.07437; J. Ren and J. H. Yu, arXiv:1602.07708; C.W. Chiang *et al.*, arXiv:1602.07909; F. Domingo *et al.*, arXiv:1602.07691; C. Han *et al.*, arXiv:1602.08100; B.A. Arbuzov and I.V. Zaitsev, arXiv:1602.08293; T. Nomura *et al.*, arXiv:1602.08302; Y. Kats and M. Strassler, arXiv:1602.08819; C. Beskidt *et al.*,

arXiv:1602.08707; T. Li *et al.*, arXiv:1602.09099; M. He *et al.*, arXiv:1603.00287; Y. Tsai *et al.*, arXiv:1603.00024; R. Barbieri *et al.*, arXiv:1603.00718; M. Backovic, arXiv:1603.01204; C.Y. Chen *et al.*, arXiv:1603.01256.

[7] A. Falkowski *et al.*, JHEP **1602**, 152 (2016) [arXiv:1512.05777]; K. Cheung *et al.*, arXiv:1512.07853.

[8] S. Fichet *et al.*, arXiv:1512.05751.

[9] C. Csaki *et al.*, Phys. Rev. D **93**, no. 3, 035002 (2016) [arXiv:1512.05776].

[10] C. Csaki *et al.*, arXiv:1601.00638.

[11] L. Berthier *et al.*, arXiv:1512.06799; J. A. Casas *et al.*, arXiv:1512.07895; T. Nomura and H. Okada, Phys. Lett. B **755**, 306 (2016) [arXiv:1601.00386]; F. D'Eramo *et al.*, arXiv:1601.01571; I. Sahin, arXiv:1601.01676; S. Fichet *et al.*, arXiv:1601.01712; M. Fabbrichesi and A. Urbano, arXiv:1601.02447; S. Abel and V. V. Khoze, arXiv:1601.07167; L. A. Harland-Lang *et al.*, arXiv:1601.07187. T. Nomura and H. Okada, arXiv:1601.07339; A. D. Martin and M. G. Ryskin, J. Phys. G **43**, 04 (2016) [arXiv:1601.07774]; N. D. Barrie *et al.*, Phys. Lett. B **755**, 343 (2016) [arXiv:1602.00475]; C. Gross *et al.*, arXiv:1602.03877; C. Frugiuele *et al.*, arXiv:1602.04822; P. Ko *et al.*, arXiv:1602.07214; E. Molinaro *et al.*, arXiv:1602.07574.

[12] V. Keus, S.F. King, and S. Moretti, JHEP **1401**, 052 (2014) [arXiv:1310.8253 [hep-ph]].

[13] A. Ahriche, G. Faisel, S.Y. Ho, S. Nasri, and J. Tandean, Phys. Rev. D **92**, no. 3, 035020 (2015) [arXiv:1501.06605 [hep-ph]].

[14] G. Aad *et al.* [ATLAS and CMS Collaborations], Phys. Rev. Lett. **114**, 191803 (2015) [arXiv: 1503.07589 [hep-ex]].

[15] S. Heinemeyer *et al.* [LHC Higgs Cross Section Working Group Collaboration], arXiv:1307.1347 [hep-ph]. Online updates available at <https://twiki.cern.ch/twiki/bin/view/LHCPhysics/CERNYellowReportPageBR2014>.

[16] C.S. Chen, C.Q. Geng, D. Huang, and L.H. Tsai, Phys. Rev. D **87**, 075019 (2013) [arXiv:1301.4694 [hep-ph]].

[17] S. Kanemura, T. Kasai, and Y. Okada, Phys. Lett. B **471**, 182 (1999) [hep-ph/9903289].

[18] M.E. Peskin and T. Takeuchi, Phys. Rev. D **46**, 381 (1992).

[19] K.A. Olive *et al.* [Particle Data Group Collaboration], Chin. Phys. C **38**, 090001 (2014) and 2015 update.

[20] W. Grimus, L. Lavoura, O.M. Ogreid, and P. Osland, Nucl. Phys. B **801**, 81 (2008) [arXiv:0802.4353 [hep-ph]].

[21] The ATLAS and CMS Collaborations, ATLAS-CONF-2015-044 and CMS-PAS-HIG-15-002.

[22] K. Cheung, P. Ko, J.S. Lee, and P.Y. Tseng, JHEP **1510**, 057 (2015) [arXiv:1507.06158 [hep-ph]].

[23] G. Aad *et al.* [ATLAS Collaboration], Phys. Rev. Lett. **113**, no. 17, 171801 (2014) [arXiv:1407.6583 [hep-ex]].

[24] V. Khachatryan *et al.* [CMS Collaboration], Phys. Lett. B **750**, 494 (2015) [arXiv:1506.02301 [hep-ex]].

[25] G. Aad *et al.* [ATLAS Collaboration], Phys. Lett. B **738**, 428 (2014) [arXiv:1407.8150 [hep-ex]].

[26] G. Aad *et al.* [ATLAS Collaboration], JHEP **1601**, 032 (2016) [arXiv:1509.00389 [hep-ex]].

[27] V. Khachatryan *et al.* [CMS Collaboration], JHEP **1510**, 144 (2015) [arXiv:1504.00936 [hep-ex]].

[28] G. Aad *et al.* [ATLAS Collaboration], Eur. Phys. J. C **76**, no. 1, 45 (2016) [arXiv:1507.05930 [hep-ex]].

[29] ATLAS Collaboration, ATLAS-CONF-2014-005.

[30] S. Chatrchyan *et al.* [CMS Collaboration], Phys. Rev. Lett. **111**, no. 21, 211804 (2013) [Phys. Rev. Lett. **112**, no. 11, 119903 (2014)] [arXiv:1309.2030 [hep-ex]].

[31] <https://twiki.cern.ch/twiki/bin/view/LHCPhysics/CERNYellowReportPageAt8TeV2014>.

- [32] <https://twiki.cern.ch/twiki/bin/view/LHCPhysics/CERNYellowReportPageAt1314TeV2014>.
- [33] J. Jaeckel, M. Jankowiak, and M. Spannowsky, Phys. Dark Univ. **2**, 111 (2013) [arXiv:1212.3620 [hep-ph]].
- [34] A. Ahriche, K.L. McDonald, and S. Nasri, arXiv:1604.05569 [hep-ph].
- [35] E. Ma, I. Picek, and B. Radovcić, Phys. Lett. B **726**, 744 (2013) [arXiv:1308.5313 [hep-ph]].
- [36] M. Aaboud *et al.* [ATLAS Collaboration], arXiv:1607.06363 [hep-ex].
- [37] CMS Collaboration [CMS Collaboration], CMS-PAS-EXO-16-020; CMS-PAS-EXO-16-021.